4-anilinoquinazoline derivatives as the first potent NOD1-RIPK2 signaling pathway inhibitors at the nanomolar range with potential anti-inflammatory activity

Amélie Barczyk,[a†] Perrine Six,[a†] Morgane Rivoal,[a] Claire Devos,[a] Xavier Dezitter,[a] Min-Jeong Cornu-Choi,[a] Karine Huard,[b] Erika Pellegrini,[b,c] Stephen Cusack,[b] Laurent Dubuquoy,[a] Régis Millet,[a] Natascha Leleu-Chavain[a*]

[a] *Univ. Lille, Inserm, CHU Lille, U1286 – INFINITE – Institute for Translational Research in Inflammation, F-59000 Lille, France*

[b] *European Molecular Biology Laboratory, 71 Avenue des Martyrs, CS 90181, 38042 Grenoble Cedex 9, France*

[c] *Current address: IBS, Grenoble France*

RECEIVED DATE (to be automatically inserted after your manuscript is accepted if required according to the journal that you are submitting your paper to)††

† These authors contributed equally *Correspondence: Dr. Natascha Leleu-Chavain, Phone, +33 3 20 96 49 93; e-mail: natascha.leleu@univ-lille.fr.

1. ABSTRACT

Inflammation is a defense mechanism that restores tissue damages and eliminates pathogens. Among the Pattern Recognition Receptors that recognize danger or pathogenic signals, Nucleotide Oligomerization Domain 1 and 2 (NOD1/2) have been identified to play an important role in innate immunity responses and inhibition of NOD1 could be interesting to treat severe infections and inflammatory diseases. In this work, we identified the first selective NOD1 *vs* NOD2 pathway inhibitors at the nanomolar range based on a 4-anilinoquinazoline scaffold. We demonstrated that NOD1 inhibition occurs through the inhibition of Receptor Interacting Protein Kinase 2 (RIPK2), involved in its downstream signaling pathways. Compound **37** demonstrates no cytotoxicity, a selectivity for RIPK2 over Epithelial and

Vascular Endothelial Growth Factor Receptors (EGFR/VEGFR) and a capacity to reduce pro-inflammatory cytokine IL-8 secretion. The structure of the RIPK2-compound **37** complex was resolved by crystallography. The 4-anilinoquinazoline scaffold offers novel perspectives to design NOD1-RIPK2 inhibitors, potentially useful to treat inflammatory diseases.

KEYWORDS: NOD1, RIPK2, inflammation, inflammatory diseases, kinase inhibitors

2. INTRODUCTION

Inflammation is a defense mechanism with the function to restore tissue damages and to eliminate pathogens. Inflammation can be sterile when triggered by danger signals (DAMP: Danger Associated Molecular Pattern) delivered from damaged cells (e.g.: cancer cells) or external factors (e.g.: pollution, UV). Inflammation can also be of infectious origin (e.g.: bacteria, virus) and then involves pathogenic signals (PAMP: Pathogen Associated Molecular Pattern). These patterns, DAMP and PAMP, are recognized by immune cells present in tissues, through Pattern Recognition Receptors (PRR). PRR activate these cells, inducing defense mechanisms by the secretion of inflammatory mediators (inflammatory cytokines, chemokines, interferons…) but also activation of cell death pathways in order to remove pathogen-infected or damaged cells.[1] Thus, immune cells are key players in the inflammation response because they act rapidly after detection of a danger.

While the Toll-Like Receptors (TLR) family constitutes the majority of PRR, Nucleotide Oligomerization Domain (NOD) Like Receptors (NLR) have been identified to play an important role in innate immunity responses. NOD proteins 1 and 2 (NOD1/2) are the most widely studied members of the NLR family. They are particularly interesting because they recognize bacterial components abnormally present in the cytoplasm derived from peptidoglycans (PGN) of bacteria and trigger various signals vital for host defense and inflammation,[2,3] including Nuclear Factor-kappa B (NF-kB), stress kinases, and Interferon Response Factors (IRFs).[4–6] NOD1 is activated by its natural ligand, γ-D-glutamyl-meso-diaminopimelic acid (ie-DAP), a dipeptide present in many Gram-negative and some Gram-positive bacteria. After NOD1 activation, the binding of Adenosine TriPhosphate (ATP) leads to auto-oligomerization of the receptor followed by the recruitment of a serine/threonine kinase, Receptor Interacting Protein Kinase 2 (RIPK2) *via* a Caspase Activation and Recruitment Domain (CARD)-CARD interaction resulting in the activation of NF-kB and Mitogen-Activated Protein Kinase (MAPK) signaling.

It has been reviewed that modulation of NOD1 could be interesting to treat severe infections and inflammatory diseases.[7] More precisely, studies have demonstrated the role of NOD1 in host defense (regulation of pulmonary and intestinal innate immunity, cancer), in cardiovascular diseases (septic shock, atherosclerosis) and in metabolic disorders. For example, involvement of NOD1 in innate host defense was highlighted in the gastrointestinal tract. It eliminates gastrointestinal pathogens and regulates inflammatory responses suggesting that NOD1 may be an interesting target to treat intestinal pathologies.[8] The role of NOD1 was also evidenced in myocardial diseases. Indeed, NOD1 is expressed in cardiac myocytes and fibroblasts and not only in immune cells.[9] When stimulated, NOD1 activates apoptotic pathways in murine cardiomyocytes and pro-fibrotic mediators in cardiac fibroblasts. Moreover, cardiac dysfunctions were observed after NOD1 activation by the synthetic ligand C12-ieDAP. Targeting NOD1 appears to be an interesting solution for inflammatory-induced cardiac diseases like heart failure. The implication of NOD1 in the insulin resistance was also reported.[10,11] Nod1 gene expression has been identified to be upregulated in conditions of metabolic dysregulation and NOD1-dependent insulin resistance has been evidenced.[12,13] It has also been demonstrated that Nod1 KO mice are protected from developing high-fat diet-induced insulin intolerance and lipid accumulation.[14,15] Regarding all these results, the development of NOD1 inhibitors would be of great interest to treat metabolic diseases. In conclusion, the implication of NOD1 signal in chronic inflammatory conditions reveals the inhibition of NOD1 as an attractive approach to reduce excessive inflammation.

Until now, only few NOD1 inhibitors have been described and only 4 chemical series have shown a selective and specific inhibition of NOD1 compared to NOD2 at the micromolar range (Figure 1).[16,17] Moreover, the mode of action of these molecules remains unclear and therapeutic potential of NOD1 inhibition is largely unexplored. Nevertheless, it has been demonstrated that ML130 (Noditinib-1) binds to the ligand binding domain of NOD1 and alters its conformation and subcellular localization.[18] Recently, the research results of Russo *et al.* are in disagreement with this first statement. They have evidenced that ML130 bind directly to the NOD1 Nucleotide-Binding Domain (NBD).[19] The NBD, which is common to all NLR, mediates oligomerization of NOD1 after ATP binding. SB711, with its purine-like structure, supposedly binds to the nucleotide-binding domain of NOD1.[20] There are several possibilities to block NOD signaling pathway. Jakopin mentioned 5 rational targeting of the NOD signaling pathway: 1. Targeting the ligand binding; 2. Targeting the ATP-binding site; 3.

Targeting the NOD self-oligomerization; 4. Targeting the RIPK2 recruitment or RIPK2 kinase activity and 5. Targeting the regulatory network of signal transduction.[20] Recently, the most described strategy to inhibit NOD signals consists in the development of specific NOD signaling pathway inhibitors, especially RIPK2 inhibitors.

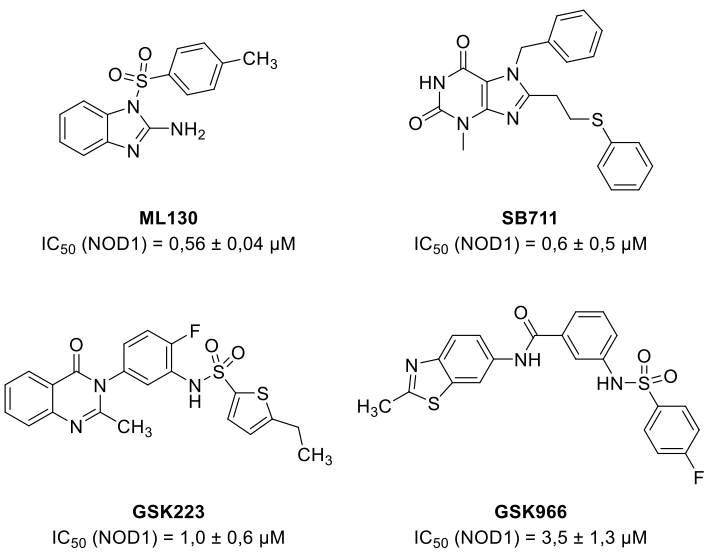

Figure 1. Chemical structure and half-maximal inhibitory concentration (IC_{50}) on NOD1 of selective NOD1 inhibitors from the literature

Identified from known kinase inhibitors, the first RIPK2 inhibitors lacked selectivity. Indeed, their activity on RIPK2 was actually an off-target effect of the molecules. Among these non-selective inhibitors, mention may be made of Gefitinib,[21] a well-known Epidermal Growth Factor Receptor (EGFR) inhibitor, or Ponatinib,[22] a Breakpoint Cluster Region-Abelson (BCR-ABL) inhibitor. More recently, more selective inhibitors of RIPK2 have been identified by Oncodesign Precision Medicine (OD), GlaxoSmithKline (GSK), Novartis or academic research groups (Figure 2) such as OD38,[21] WEHI-345,[23] compound **1**,[24] GSK583,[25] compound **2**,[26] compound **3**,[27] CLSP37,[28] UH15-15,[29] or BI 706039 (structure unknown).[30] The molecules delay the activation of the NF-kB pathway induced by NOD. End of 2019, the biopharmaceutical group Oncodesign has identified a new drug candidate first-in-class, ODS 101 (structure unknown), a selective RIPK2 inhibitor with a strong potential in the treatment of auto-immune and inflammatory diseases and more precisely Inflammatory Bowel Diseases (IBD). Toxicologic preclinical assays have been successfully achieved demonstrating the therapeutic potential of RIPK2 inhibitors.[31] Based on these recent discoveries, we decided to develop NOD1-RIPK2 inhibitors for the treatment of inflammatory diseases.

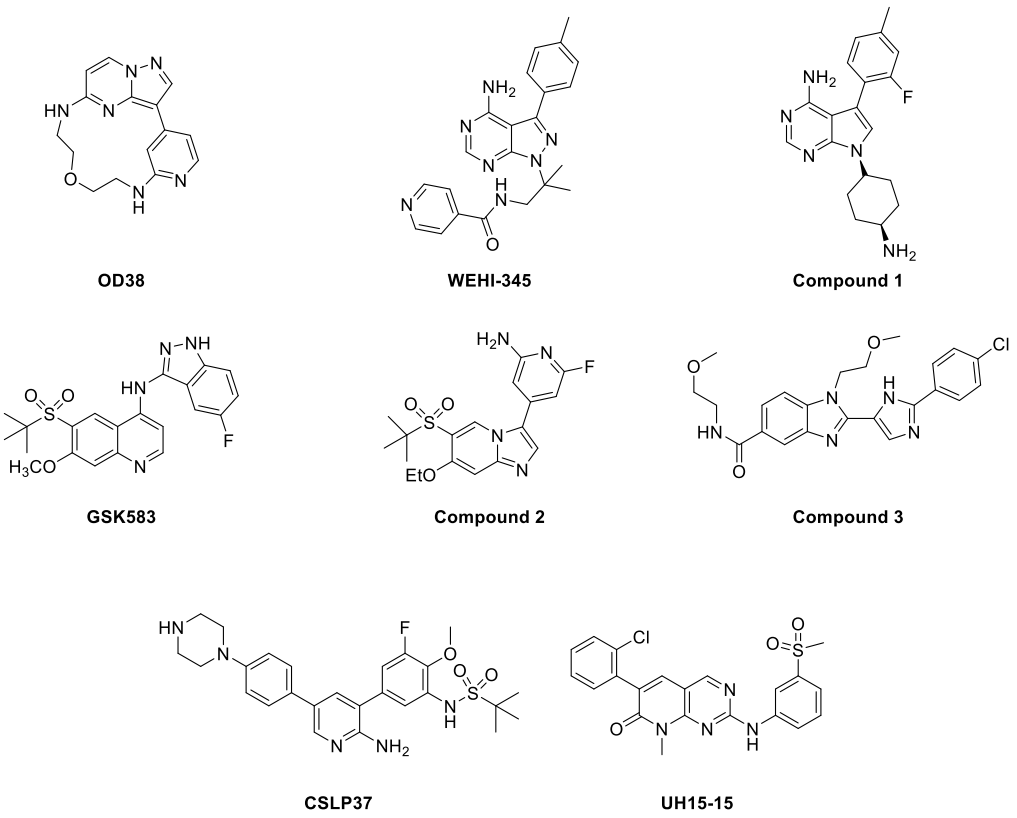

Figure 2. Chemical structure of RIPK2 inhibitors from the literature

To identify inhibitors of NOD1 signaling, a screening of our chemical library was carried out on Human Embryonic Kidney (HEK)-Blue™-*h*NOD1 cells, stably expressing human NOD1 and a NF-kB driven SEAP reporter gene. Our screening resulted in the identification of one hit with a half-maximal Inhibitory Concentration (IC_{50}) of 106 ± 28.64 nM (Figure 3, compound **4**). Compound **4** was initially designed in a previous research program to target EGFR/VEGFR. Given its origin, compound **4** was evaluated on RIPK2 and showed a capacity to inhibit RIPK2 with an IC_{50} value of 1.21 ± 0.57 nM. Starting from this molecule, we investigated the synthesis and Structure-Activity Relationship (SAR) of a series of quinazoline derivatives. Thirty new quinazolines were synthesized and tested for their capacity to inhibit the NOD1 pathway. Selectivity towards NOD1 *vs* NOD2 and specificity compared to the Tumour Necrosis Factor-alpha (TNFα) pathway was evaluated. Identified selective NOD1 inhibitors were tested for their capacity to inhibit RIPK2. Selectivity of our NOD1-RIPK2 inhibitors over EGFR and VEGFR was also determined. Finally, the anti-inflammatory activity of our best compound was evaluated through their capacity to decrease pro-inflammatory cytokine IL-8 secretion in HEK-Blue™-*h*NOD1.

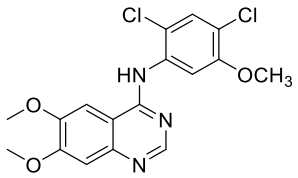

Compound 4

Figure 3. Chemical structure of our hit compound identified by screening on HEK-Blue™-*h*NOD1 cells.

3. RESULTS AND DISCUSSION

a. Chemistry.

Four series of compounds, differentiated by the ether substituent (methoxy, methoxyethoxy or diethylaminoethoxy) at the *C*-6, *C*-7 and *C*-8 positions of the quinazoline core (R_1, R_2 and R_3), and the aniline at the *C*-4 position (R_4), were synthesized (Figure 4).

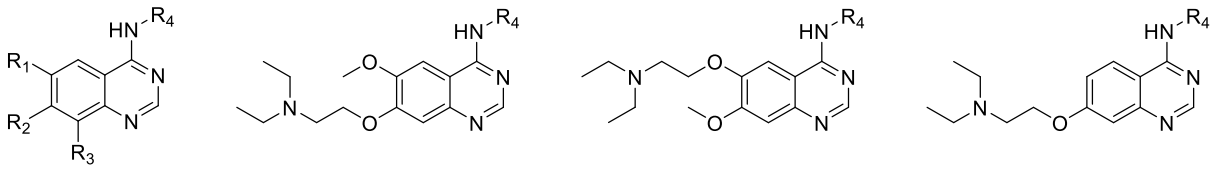

A series **B series** **C series** **D series**

Figure 4. General chemical structure of our four series of quinazolines.

The synthesis of the A series is illustrated in Scheme 1. Commercially available 4-chloroquinazoline derivatives **1-3** were engaged in a nucleophilic substitution reaction in the presence of various commercial anilines in 2-propanol at reflux (method a) or in DMF in the presence of sodium hydride (60%) at 50°C (method b) to obtain the final products **4-31**.

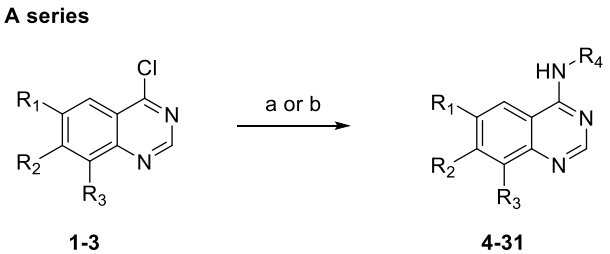

Scheme 1. Synthesis of compounds **4-31** (A series)
Reagents and conditions: (a) aniline R_4-NH_2, isopropyl alcohol, reflux; (b) aniline R_4-NH_2, NaH, DMF, 50 °C.

Compounds **37** (B series) and **43** (C series) were synthesized in 6 steps (Scheme 2). First, the phenol function of methyl vanillate and methyl 3-hydroxy-4-methoxybenzoate was alkylated with 2-diethylaminoethyl chloride hydrochloride in presence of potassium carbonate in acetone

at reflux for 3h to obtain the intermediate compounds **32** and **38**, respectively (76% and 77% yield, respectively). These intermediates were nitrated in the presence of a mixture of nitric acid and tin tetrachloride in dichloromethane at -70°C for 4h.[32] Nitration occurs selectively at the 2-position due to electronic effects of the different substituents on the benzene ring. The position of the nitro group was confirmed by ^{1}H NMR. The nitro derivatives **33** and **39** were obtained with good yield (88-91%). Catalytic hydrogenation of the nitro group in the presence of Raney®-nickel in methanol led to amino derivatives **34** and **40** (66-77% yields), which were converted by cyclization with formamide in the presence of ammonium formate at 140°C for 16h to obtain the cyclized compounds **35** and **41** with good yields (68-71%). Finally, cyclized compounds were reacted with phosphorus oxychloride at 120°C for 2h to obtain the intermediate 4-chloroquinazolines **36** and **42** (95% and 92% yield, respectively). Finally, the desired quinazolines **37** (B series) and **43** (C series) were obtained as described previously for the A series.

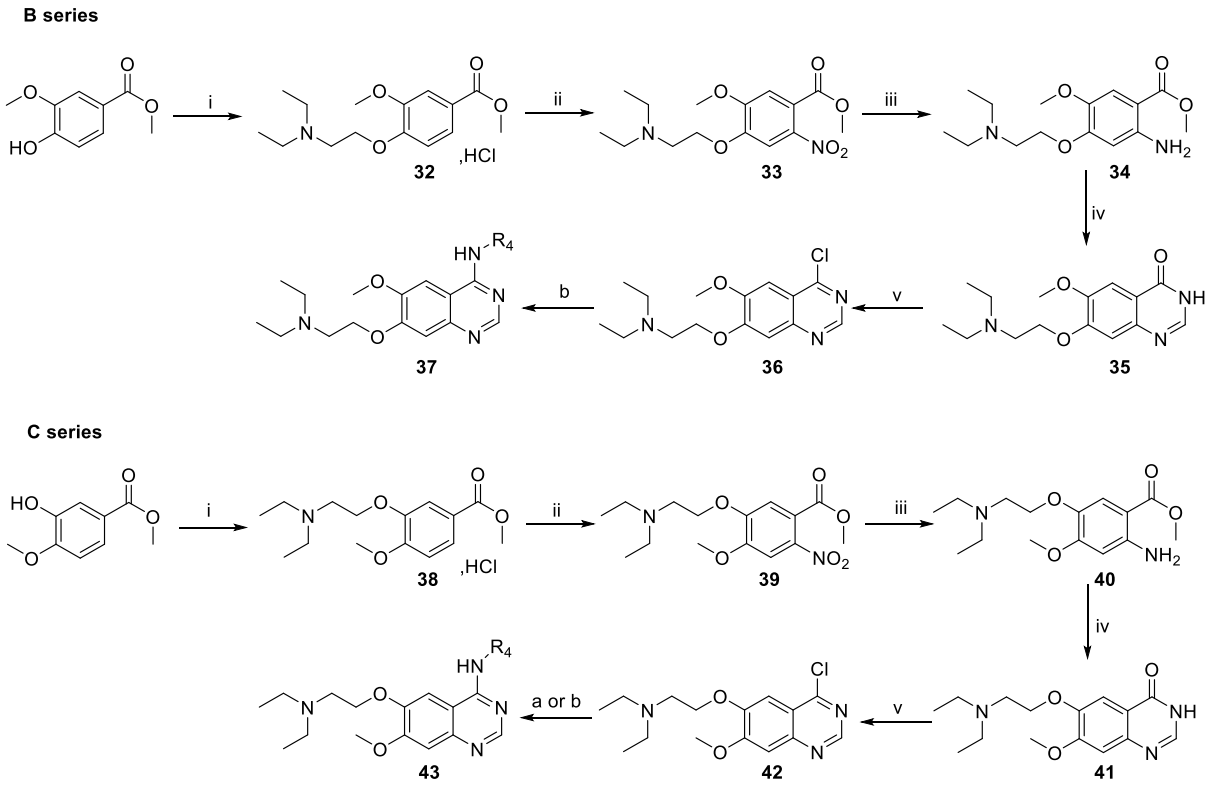

Scheme 2. Synthesis of compounds **37** (B series) and **43** (C series)
Reagents and conditions: (i) $ClCH_2CH_2N(CH_2CH_3)_2.HCl$, K_2CO_3, acetone, reflux, 3h; (ii) $SnCl_4$, HNO_3, CH_2Cl, -25°C,4h; (iii) Raney Ni, H_2, MeOH, rt, 16h; (iv) $HCOONH_4$, $HCONH_2$, 140°C, 16h; (v) $POCl_3$, 120°C, 2h; (a) aniline R_4-NH_2, isopropyl alcohol, reflux; (b) aniline R_4-NH_2, NaH, DMF, 50 °C.

As depicted in Scheme 3, compound **47** was prepared starting from the commercial methyl 2-amino-4-hydroxybenzoate in four steps. The intermediate compounds **44**, **45** and **46** were

obtained using the same procedure as described for the B and C series. Compound **47** was obtained using method b with 16% yield.

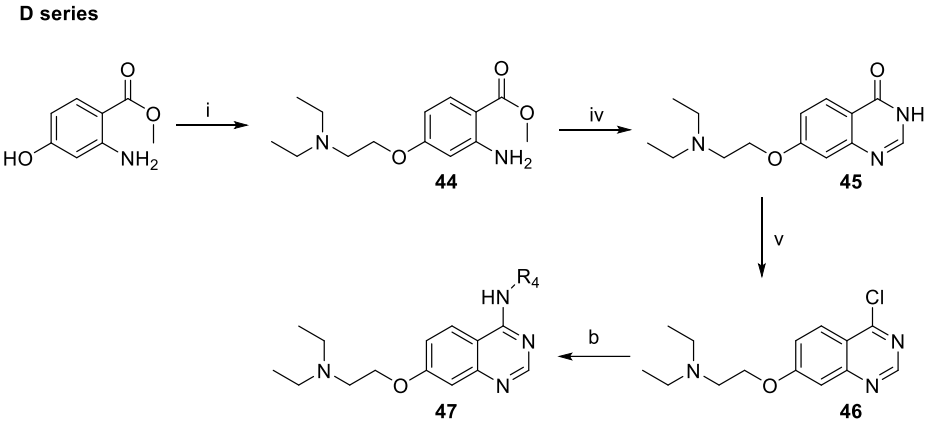

Scheme 3. Synthesis of compound **47** (D series)
Reagents and conditions: (i) $ClCH_2CH_2N(CH_2CH_3)_2.HCl$, K_2CO_3, acetone, reflux, 3h; (iv) $HCOONH_4$, $HCONH_2$, 140°C, 16h; (v) $POCl_3$, 120°C, 2h; (b) aniline R_4-NH_2, NaH, DMF, 50 °C.

b. **Structure-activity relationships**.

We chose to first screen the new synthesized molecules on HEK-Blue™-*h*NOD1 cells since our main objective is to discover NOD1 inflammatory pathway inhibitors. A screening on RIPK2 directly seemed less judicious to us given that several highly potent RIPK2 inhibitors blocked only slightly NOD pathway,[28] thereby reducing their potential for the treatment of inflammatory diseases. We started our pharmacomodulations from the hit compound **4** identified during the initial screening procedure. This quinazoline, with an IC_{50} value of 106 ± 28.64 nM, is a potent NOD1 inhibitor. From this compound, we modulated the aniline (R_4) at position 4 of the quinazoline core to establish SAR (Tables 1 and 2).

First, we decided to evaluate the importance of each substituent of the 2,4-dichloro-5-methoxyaniline of the starting hit compound (Table 1). When one or more of these substituents are removed, the capacity of the molecule to inhibit the NOD1 pathway is reduced or even completely lost (compounds **5-9**). We also studied the position of the chlorine atoms. Their position influences the inhibitory activity of the molecule on NOD1. Compound **5** bearing 2 chlorine atoms at positions 2 and 4 of the aniline lost its capacity to inhibit the NOD1 pathway. However, when these 2 chlorine atoms are at positions 4 and 5 (compound **10**), a modest activity is observed (IC_{50} = 355 ± 48 nM). In the same way, compound **8** with a chlorine atom at position

4 of the aniline has a modest activity on NOD1 (IC_{50} = 283 ± 3 nM) whereas compound **11** with a chlorine atom at position 5 of the aniline completely lost its activity.

Table 1: Synthesized 4-anilino-6,7-dimethoxyquinazolines, their capacity to inhibit the NOD1 pathway in HEK-Blue™-*h*NOD1 cells (IC_{50} (NOD1)), the NOD2 pathway in HEK-Blue™-*h*NOD2 (IC_{50} (NOD2)) and their specificity toward the TNF pathway in HEK-Blue™-*h*NOD1 cells (IC_{50} (TNFα)).

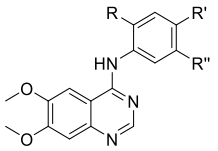

Compounds	R	R'	R''	IC_{50} (NOD1) nM	IC_{50} (NOD2) nM	IC_{50} (TNFα) nM
4	Cl	Cl	OCH_3	106 ± 28.64	>10 000	>10 000
5	Cl	Cl	H	>10 000	>10 000	>10 000
6	H	Cl	OCH_3	>10 000	>10 000	>10 000
7	Cl	H	OCH_3	686 ± 58	>10 000	>10 000
8	H	Cl	H	283 ± 3	>10 000	>10 000
9	Cl	H	H	>10 000	>10 000	>10 000
10	H	Cl	Cl	363 ± 37	>10 000	>10 000
11	H	H	Cl	>10 000	>10 000	>10 000
12	Br	H	Br	>10 000	>10 000	>10 000
13	H	F	Cl	1344 ± 764	>10 000	>10 000
14	F	Br	H	549 ±139	>10 000	>10 000
15	F	Br	OCH_3	220 ± 54	>10 000	>10 000
16	Cl	Cl	OH	>10 000	>10 000	>10 000
17	H	Cl	OH	33 ± 4.4	>10 000	>10 000
18	H	H	OH	157 ± 2.83	>10 000	>10 000
19	H	Br	OH	>10 000	>10 000	>10 000
20	H	F	OH	81 ± 38	>10 000	>10 000
21	H	Cl	NH_2	36.69 ± 4.20	>10 000	>10 000
22	H	H	NH_2	>10 000	>10 000	>10 000
23	H	H	H	>10 000	>10 000	>10 000
ML130				1830 ± 355	>10 000	>10 000

Data are mean ± SEM of three experiments performed in duplicates.

The nature of the halogens also influences the capacity of the molecule to inhibit NOD1 pathway (Table 1). The replacement of the chlorine atom at position 4 of the aniline of compound **10** by a fluorine atom induces a loss of activity (compound **13**). On the other hand, if the 2 chlorine atoms at positions 2 and 4 of the aniline of compound **5** are replaced by a

fluorine atom and a bromine atom, respectively (compound **14**), a slight gain of activity was observed. Thus, we substituted the chlorine atoms of compound **4** by fluorine and bromine atoms at positions 2 and 4, respectively (compound **15**) but we did not observe the expected gain of activity on NOD1 (IC_{50} = 220 ± 54 nM).

The replacement of the methoxy group of compound **4** by a hydroxyl group induces a total loss of activity (Table 1, compound **16**). Surprisingly, if the chlorine atom at position 2 of compound **16** is removed (compound **17**), the molecule shows a better activity than compound **4** (IC_{50} = 33 ± 4.4 nM). The removal of the second chlorine atom helps to maintain good activity on NOD1 (compound **18**, IC_{50} = 157 nM), however not as good as compound **16** with one chlorine atom left. Once again, the nature of the halogen influences the activity of the molecule on NOD1. A replacement of the chlorine atom of compound **17** by a bromide atom (compound **19**) induces a total loss of activity while its replacement by a fluorine atom affords compound **20** to retain a good activity on NOD1 slightly lower to the one of compound **17** (IC_{50} = 81 ± 38 nM).

The substitution of the hydroxyl function of compound **17** by an amine function allows compound **21** to maintain a good capacity to inhibit the NOD1 pathway (IC_{50} = 36.69 ± 4.20 nM) when the chlorine atom is conserved at position 4 (Table 1). However, when the molecule only bears an amine function at position 5, the capacity of compound **22** to inhibit NOD1 drops sharply.

All identified NOD1 inhibitors were tested on HEK-Blue™ cells expressing human NOD2 (HEK-Blue™-*h*NOD2) and stimulated with the NOD2 agonist muramyl dipeptide (MDP). Our compounds did not alter NOD2 signaling and showed markedly selectivity for NOD1 *vs* NOD2. Specificity of identified NOD1 inhibitors was also evaluated on HEK-Blue™-*h*NOD1 cells stimulated by TNFα. None of the compounds interfered with TNFα signaling and they all showed good specificity for the NOD1 pathway *vs* the TNFα pathway.

The activity of our compounds on NOD1 was compared with that of ML130, a well-known selective NOD1 inhibitor from the literature. We demonstrated that our NOD1 inhibitors are more active than ML130. Especially, our best compound **17** is 55 times more active than ML130 on the NOD1 pathway. Herein, we described the first selective NOD1 inhibitors active at the nanomolar range.

Table 2: Synthesized 4-aryl-6,7-dimethoxyquinazolines, their capacity to inhibit the NOD1 pathway in HEK-Blue™-*h*NOD1 cells (IC_{50} (NOD1)), the NOD2 pathway in HEK-Blue™-*h*NOD2 (IC_{50} (NOD2)) and their specificity toward the TNF pathway in HEK-Blue™-*h*NOD1 cells (IC_{50} (TNFα)).

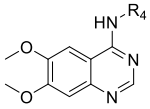

Compounds	R_4	IC_{50} (NOD1) nM	IC_{50} (NOD2) nM	IC_{50} (TNFα) nM
4	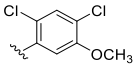	106 ± 28.64	>10 000	>10 000
24	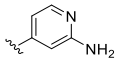	>10 000	>10 000	>10 000
25		>10 000	>10 000	>10 000
26		>10 000	>10 000	>10 000
27	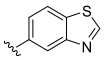	41.71 ± 8.38	>10 000	>10 000
28	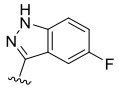	228 ± 10	>1 000	>10 000
29	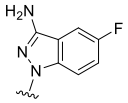	>10 000	>10 000	>10 000
ML130		1830 ± 355	>10 000	>10 000

Data are mean ± SEM of three experiments performed in duplicates.

Different aromatic amines were also introduced at position 4 of the quinazoline (Table 2). These aromatic amines were chosen from the chemical structures of RIPK2 inhibitors described in the literature [25,26,33]. Replacing an aniline with a benzothiazole affords compound **27** with a good capacity to inhibit NOD1 pathway (IC_{50} = 41.71 ± 8.38 nM). This molecule maintains proper selectivity for NOD1 *vs* NOD2. When the aniline is substituted with a 5-fluoro-1*H*-indazol-3-amine (compound **28**), moderate activity on NOD1 is retained (IC_{50} = 228 ± 10 nM). Moreover, this molecule is less selective (SI = 7.5). All other attempts to substitute the aniline group by another aromatic group failed.

Table 3: Synthesized 4-(2,4-dichloro-5-methoxyanilino)-6,7-alkoxyquinazolines, their capacity to inhibit the NOD1 pathway in HEK-Blue™-*h*NOD1 cells (IC_{50} (NOD1)), the NOD2 pathway in HEK-Blue™-*h*NOD2 (IC_{50} (NOD2)) and their specificity toward the TNF pathway in HEK-Blue™-*h*NOD1 cells (IC_{50} (TNFα)).

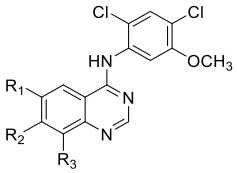

Compounds	R_1	R_2	R_3	IC_{50} (NOD1) nM	IC_{50} (NOD2) nM	IC_{50} (TNFα) nM
4			H	106 ± 28.64	>10 000	>10 000
30	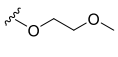	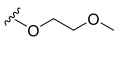	H	101 ± 35	>10 000	>10 000
37		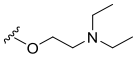	H	41.57 ± 7.93	>1 000	>10 000
43	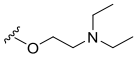		H	153 ± 17	>10 000	>10 000
47	H	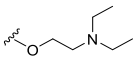	H	>10 000	>10 000	>10 000
31				>10 000	>10 000	>10 000
ML130				1830 ± 355	>10 000	>10 000

Data are mean ± SEM of three experiments performed in duplicates.

Then, we decided to modulate the substitution of the quinazoline core: R_1, R_2 and R_3 (Table 3). First, replacing both methoxy groups of compound **4** by methoxyethoxy groups (compound **30**) has no influence on the activity on NOD1: compound **30** maintains a capacity to inhibit NOD1 pathway in the same range as the hit molecule. Each methoxy group of compound **4** was also replaced by a 2-diethylaminoethoxy chain either at position 6 (R_1) or at position 7 (R_2) (compounds **37** and **43**). If the 2-diethylaminoethoxy chain is introduced at position 7 of the quinazoline (compound **37**), a gain in activity on NOD1 of the molecule is observed (IC_{50} = 41.57 ± 7.93 nM) with a slight decrease in selectivity. If this same chain is introduced at position 6 (compound **43**), the activity on NOD1 is slightly reduced (IC_{50} = 153 ± 17 nM) and good selectivity is maintained. On the other hand, if this chain is maintained at position 7 but the methoxy group at position 6 is removed, compound **47** lost all activity on NOD1. The introduction of a third methoxy group at position 8 (R_3, compound **31**) induces a total loss of activity on NOD1.

4. RIPK2 inhibition.

When activated, NOD1 recruits RIPK2, leading to the activation of NF-kB and MAPK pathways [34]. Thus, we wanted to check if our molecules inhibit the NOD1 pathway through the inhibition of RIPK2. For this purpose, our best NOD1 inhibitors in HEK-Blue™-*h*NOD1 (IC_{50} (NOD1) < 100 nM) were evaluated on an ADP-Glo™ RIPK2 assay, a luminescent kinase assay measuring ADP formed when the kinase is activated. The formed ADP is then converted into ATP, which is also converted into light by Ultra-Glo™ luciferase. The luminescence correlates with the quantity of ADP produced and therefore with RIPK2 activity.

All our NOD1 signaling inhibitors showed an excellent capacity to inhibit RIPK2 kinase activity with IC_{50} at the low nanomolar range (0.65-2.07 nM), suggesting their capacity to inhibit NOD1 pathway is mediated by RIPK2 (Table 5). Our molecules showed a better inhibition capacity than gefitinib, a RIPK2 inhibitor from the literature with a quinazoline structure as well (compound **17**, our best RIPK2 inhibitor, is about 8 times more active).

Table 5: Capacity of our best NOD1 inhibitors (IC_{50} (NOD1) < 100 nM) to inhibit RIPK2.

	IC_{50} (nM)					SI	
Compounds	NOD1	NOD2	RIPK2	EGFR	VEGFR	EGFR/ RIPK2	VEGFR /RIPK2
4	106 ± 28.64	>10 000	1.21 ± 0.57	61.27 ± 3.82	>1 000	50.6	>1 000
17	33 ± 4.4	>10 000	0.65 ± 0.15	0.84 ± 0.49	1.39 ± 0.79	1.3	2.1
20	81 ± 38	>10 000	1.72 ± 0.41	2.55 ± 1.12	3.02 ± 0.98	1.5	1.7
21	36.69 ± 4.20	>10 000	1.44 ± 0.27	0.46 ± 0.23	4.09 ± 1.47	0.3	2.8
27	41.71 ± 8.38	>10 000	2.07 ± 0.93	35.69 ± 5.53	6.69 ± 2.13	17.2	3.3
37	41.57 ± 7.93	>1 000	1.52 ± 0.91	>1 000	>1 000	>1 000	>1 000
Gefitinib	605 ± 60	1080 ± 199	5.58 ± 1.14	0.72 ± 0.48	>1 000	0.1	>1 000
ML130	1830 ± 355	>10 000	>1 000	-	-	-	-

Data are mean ± SEM of three experiments performed in duplicates.

Gefitinib is a non-selective RIPK2 inhibitor and is well known as an EGFR inhibitor. Thus, we decided to evaluate our best NOD1-RIPK2 inhibitors on an ADP-Glo™ EGFR assay. Our compounds showed different results on EGFR depending on their structure. Compounds **17**, **20** and **21** demonstrated no selectivity for RIPK2 *vs* EGFR. When the aniline group at position 4 of the quinazoline core of these molecules is replaced by a benzothiazole substituent (compound **27**), the molecule becomes slightly selective for RIPK2 *vs* EGFR. When a 2,4-dichloro-5-methoxyaniline is introduced at the same position (compound **4**), the molecule displays higher

selectivity towards RIPK2 *vs* EGFR (SI = 50.6). When the methoxy group at position 7 is replaced by a 2-diethylaminoethoxy chain maintaining the 2,4-dichloro-5-methoxyaniline at position 4 (compound **37**), the selectivity is drastically increased (SI > 1000 nM), suggesting that the long chain has an impact on the selectivity of the molecule on RIPK2 *vs* EGFR.

Since there is a close connection between EGFR and VEGFR pathways [35], we also tested our compounds on an ADP-Glo™ VEGFR assay. Even though they were the only ones, compounds **4** and **37** showed excellent selectivity towards RIPK2 vs VEGFR (SI>1000). According to these results, we can suggest that the 2,4-dichloro-5-methoxyaniline at position 4 has an impact on the selectivity on RIPK2 *vs* VEGFR.

Out of curiosity, we evaluated gefitinib on HEK-Blue™-*h*NOD1 and HEK-Blue™-*h*NOD2 cells (Table 5). Despite its good capacity to inhibit RIPK2 at the nanomolar range, gefitinib showed only a weak activity on NOD1 pathway. This confirms that potent RIPK2 inhibitors do not always have a potential as potent NOD inflammatory pathway inhibitors. Our RIPK2 inhibitors have a better capacity to inhibit the NOD1 pathway than gefitinib. Moreover, they are selective for NOD1 *vs* NOD2 unlike gefitinib, which does not show any selectivity (SI (NOD2/NOD1) = 1.8). The NOD1 inhibitor ML130 was also evaluated on the ADP-Glo™ RIPK2 assay and showed no capacity to inhibit this kinase. This result is in accordance with the literature: inhibition of NOD1 pathway by ML130 is not mediated by RIPK2.[19]

5. Pro-inflammatory cytokine IL-8 secretion decrease.

With the aim to identify new anti-inflammatory compounds, we evaluated the capacity of our best molecules to decrease the level of pro-inflammatory cytokine IL-8 in HEK-Blue™-*h*NOD1 cells after stimulation with C12-iE-DAP. Compound **37** was tested at increased concentrations from 0.01 to 1 µM (Graph 1). Our molecule decreased significantly the secretion of IL-8 even at low concentration compared to non-treated cells (from about 1000 pg/mL to 750 pg/mL at 0.01 µM and 400 pg/mL at 0.5 and 1 µM). On the other hand, ML130, a NOD1 inhibitor from the literature with no capacity to inhibit RIPK2, does not decrease the secretion of IL-8. These results are very encouraging. They demonstrate the anti-inflammatory potential of our quinazolines and suggest the necessity to target RIPK2 to obtain an anti-inflammatory effect.

Graph 1: Capacity of our NOD1-RIPK2 inhibitor **37** to decrease the level of pro-inflammatory cytokine IL-8 secretion in HEK-Blue™-*h*NOD1 cells in comparison with ML130, a NOD1 inhibitor from the literature. HEK-Blue™-*h*NOD1 cells were stimulated by C12-iE-DAP at a concentration of 1000 ng/mL. ML130 was evaluated at increased concentrations from 0.01 to 1 µM and compound **37** from 0.001 to 1 µM. Data are mean ± SEM of three experiments performed in duplicates. Results were compared to C12-iE-DAP + DMSO and analysed by t test using Graphpad Prism software. $P < 0.05$ was considered significant. ns, non-significant.

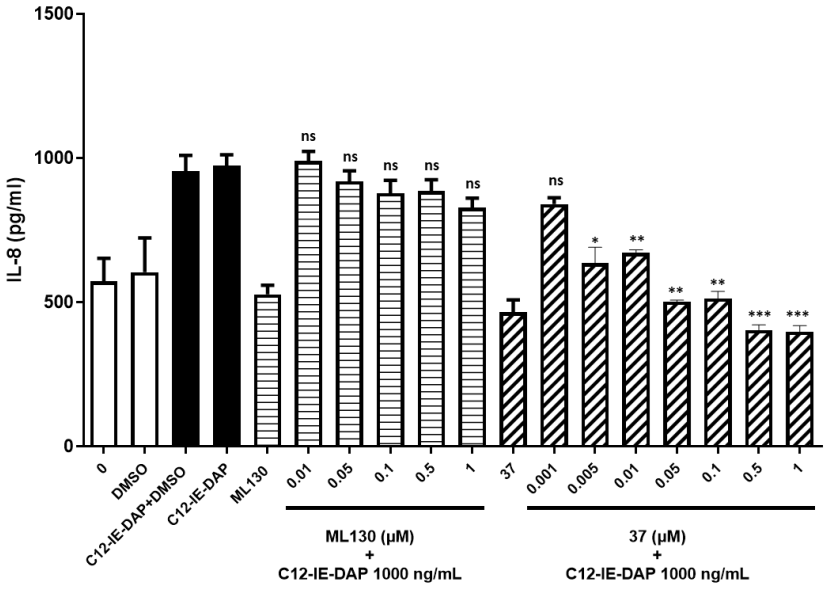

6. Cytotoxicity.

Cytotoxicity of our best compounds was evaluated using CellTiter 96® AQueous One Solution Cell Proliferation Assay, based on cell bioreduction of 3-(4,5-dimethylthiazol-2-yl)-5-(3-carboxymethoxy-phenyl)-2-(4-sulfophenyl-2*H*-tetrazolium) (MTS) to a formazan derivative. The cytotoxicity was evaluated at a concentration of 1 µM of inhibitor on HEK-Blue™-*h*NOD1, Huh7 and THP1-Blue™ NF-kB cells (Graph1, Supporting informations). All the tested compounds showed no cytotoxicity on these cell lines.

7. Structure determination of phosphorylated RIPK2 bound to compound 37.

In the aim to observe how our compounds interact with RIPK2, a crystal structure of RIPK2 bound to compound **37** was determined. To achieve this, the wild-type RIPK2 construct (residues 1-317) was used. RIPK2 becomes auto-phosphorylated when expressed in insect cells and thus corresponds to the activated form. Here, we present the structure of RIPK2 bound to compound **37**.

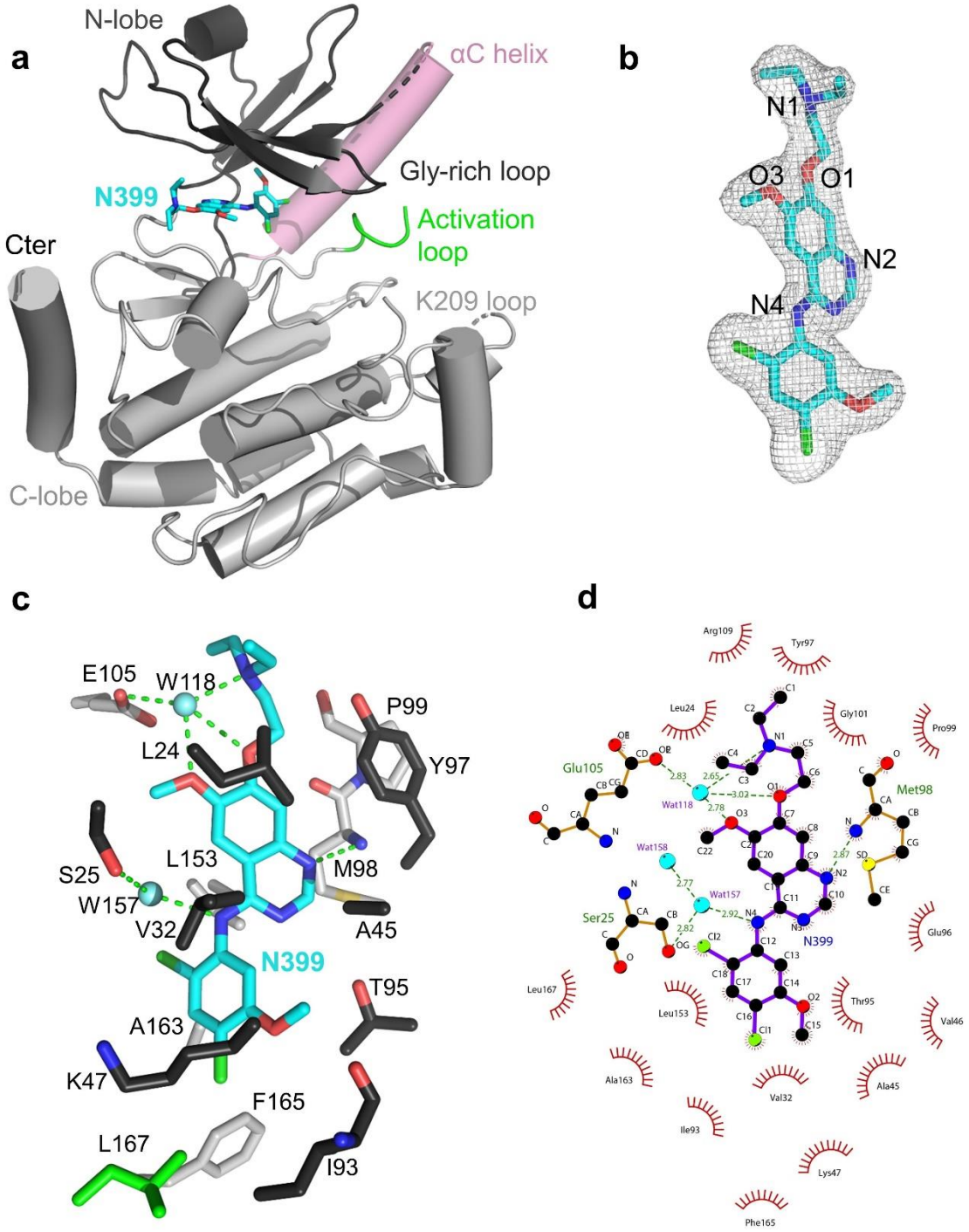

Figure 4. Structure of the RIPK2-compound **37** complex. **(a)** Ribbon representation of chain A with the kinases lobes colored in dark (N-lobe) and light grey (C-lobe), the Gly-rich loop in yellow, the activation loop in green and the K209 loop also annotated. **(b)** 2Fo-Fc map showing density for compound **37** bound to chain B with nitrogen atoms involved in hydrogen bonding labelled. **(c)** The binding site of compound **37** (chain B) showing residues in van der Walls contact (for clarity only the top side of the cavity) and forming hydrogen bonds (green dotted lines) with the inhibitor. The red spheres are water molecules. **(d)** Schematic of the interactions of compound **37** with RIPK2.

The RIPK2-compound **37** complex crystallized in space group $P2_12_12_1$ and the crystals diffracted slightly anisotropically to a maximum of ~1.9 Å resolution. Here, we describe a structure of the RIPK2-compound **37** complex determined at a maximum of 1.94 Å resolution. Two molecules (denoted chains A and B) of the kinase domain of RIPK2 (residues 1-317) form an antiparallel dimer in the asymmetric unit of the crystal. The conformation of both chains corresponds to the kinase inactive state, as previously seen in the structure of $RIPK2^{K47R}$ (PDB:5NG3)(Pellegrini et al, 2017)(Figure 5a).[36] The C-Helix is in the out-conformation and the β-sheet interaction at the N-termini is absent. The activation loop is mainly disordered.

Both chains show compound **37** bound in the kinase nucleotide-binding site in an identical fashion, although chain B is better ordered so is described here (Figure 5a-d). The extended compound **37** fits in a largely hydrophobic channel between the two lobes, bounded on the top by Leu24, Val32, Ala45, Lys47, Tyr97 and Leu167 and on the bottom by Leu79, Thr95, Met98, Gly101, Glu105, Leu153, Ala163 and Phe105 (Figure 5c,d). The compound makes one direct and four water mediated hydrogen bond to the protein (Figure 5c,d). The N2 nitrogen (for atom names see Figure 5b) forms a hydrogen bond with the amine group of Met98. The N1, O1 and O3 atoms co-ordinate a water molecule, which also forms a hydrogen bond with Glu105. The N4 nitrogen of the inhibitor indirectly engages Ser25 (a specific target residue for this particular kinase) *via* a water molecule.

8. CONCLUSION

Thirty new quinazolines have been synthesized, leading to the discovery of 15 NOD1-RIPK2 signaling inhibitors in the nanomolar range selective *vs* NOD2 and specific *vs* TNFα pathway. Pharmacomodulations were carried out and allowed to identify essential structural elements for NOD1 pathway inhibition. Compounds bearing a chlorine or a fluorine atom at position 4 and a hydrogen bond acceptor/donor like a hydroxyl group or an amine at position 3 on the aniline give the best NOD1 signaling inhibition. The replacement of the aniline by a benzothiazole is also favorable for a good inhibition. When methoxy or methoxyethoxy groups are present at positions 6 and 7 of the quinazoline, compounds demonstrated a good NOD1 pathway inhibition capacity. This inhibition was increased when a 2-diethylaminoethoxy chain was introduced at position 7 of the quinazoline. These molecules represent the first selective NOD1 signaling inhibitors at the nanomolar range. Our compounds demonstrate selectivity towards NOD1 over NOD2. Several hypotheses could explain this phenomenon. According to the

297 crystal structure of compound **37** bound to RIPK2, our inhibitors occupy the active site of
298 RIPK2 and bind its inactive state. We suppose that this interaction may lead to conformational
299 changes that allow the kinase to interfere with NOD1 pathway, but not NOD2. Indeed, the
300 cascade of event leading to NOD inflammatory pathway inhibition involves NOD1/NOD2
301 oligomerization, RIPK2 recruitment and filament formation [37] as well as subsequent
302 recruitment of E3 ligases, such as XIAP or LUBAC, to induce ubiquitination of RIPK2 and
303 activation of downstream signaling pathways.[28,38,39] A compound-induced conformational
304 change could very well interfere with this chain of event for one of the NLR and not the other.
305 Regarding RIPK2 recruitment, it was shown that different CARD-CARD interactions were
306 made between RIPK2 and NOD1/NOD2, that does not involve the same amino acids of
307 RIPK2.[40,41] Mayle *et al.* showed that the NOD1-RIPK2 pathway is very complex:
308 recruitment of RIPK2 is not sufficient for signaling activation, and the NOD1-RIPK2
309 interaction is established by multiple CARD-CARD interfaces. NOD2 differs from NOD1 by
310 the presence of 2 CARD domains. Fridh and Rittinger demonstrated that the tandem CARDs
311 of NOD2 established an intramolecular interaction and form a binding surface to interfere with
312 RIPK2, different than with a single CARD. Further investigations will be considered to unravel
313 the mechanism of NOD1-RIPK2 selectivity of our compounds.

314 Our 6 best NOD1 signaling inhibitors (IC_{50} (NOD1) < 100 nM) were able to inhibit RIPK2, a
315 Ser/Thr kinase recruited by NOD1 after its activation, at the low nanomolar range. Moreover,
316 compounds **4** and **37** showed a selectivity for RIPK2 *vs* EGFR and VEGFR unlike most
317 quinazolines in the literature. Our results suggest that the 2,4-dichloro-5-methoxyaniline at
318 position 4 is responsible for the selectivity of compound **4** *vs* VEGFR and the 2-
319 diethylaminoethoxy chain at position 7 of the quinazoline core for the additional selectivity of
320 compound **37** *vs* EGFR. Compound **37** also decreased the level of pro-inflammatory cytokine
321 IL-8 in HEK-Blue™-*h*NOD1 cells demonstrating its anti-inflammatory effect. This molecule
322 is even more efficient than the described NOD1 inhibitor ML130. In addition, the capacity of
323 our quinazolines to inhibit RIPK2 appears to be important for their anti-inflammatory activity.
324 Thus, our molecules seem interesting to treat NOD1-related inflammatory diseases. The RIPK2
325 selectivity *vs* EGFR and VEGFR is important to limit the off-target effects. However, our mixed
326 kinase inhibitors would be interesting for the treatment of the colorectal cancer as EGFR and
327 VEGFR inhibition is a well-known therapeutic approach [42,43]. RIPK2 has also been recently
328 identified as a promising therapeutic target for several types cancers [44–46] and more

encouragingly, the use of RIPK2 inhibitors for the treatment of colorectal cancer was highlighted. [47].

These first results are very promising but further pharmacomodulations are required to better understand the SAR and improve our compounds kinase selectivity.

9. EXPERIMENTAL SECTION

Cell culture (HEK-Blue™-*h*NOD1, HEK-Blue™-*h*NOD2, THP1-Blue™ NF-kB cells and Huh-7 cells). HEK-Blue™-*h*NOD1 and *h*NOD2 cells (Invivogen) were cultured in DMEM Glutamax medium (Life Technologies) with 10 % heat-deactivated FBS (Life Technologies), 1% penicillin-streptomycin (Life Technologies). All subsequent passages were cultured in the medium supplemented with 100 µg/mL Normocin, 30 µg/mL Blasticidin and 100 µg/mL Zeocin (Invivogen). The experiments were carried out on passages 7-12. THP1-Blue™ NF-kB cells (Invivogen) were cultured in RPMI 1640 Glutamax medium (Life Technologies) with 25 mM HEPES, 10 % heat-deactivated FBS (Life Technologies), 1% penicillin-streptomycin (Life Technologies). All subsequent passages were cultured in the medium supplemented with 100 µg/mL Normocin, 10 µg/mL Blasticidin (Invivogen). Huh-7 cells (ATCC) were cultured in DMEM Glutamax medium (Life Technologies) with 10 % heat-deactivated FBS (Life Technologies), 1% penicillin-streptomycin (Life Technologies).

Cell Proliferation Assay. In the cell proliferation assay, HEK-Blue™-*h*NOD1 and Huh-7 cells (3000 cells/well) were seeded in triplicates on 96 well plates in 100 µL culture medium and incubated for 24 h. For THP1-Blue™ NF-kB cells, 30 000 cells/well were seeded in triplicates on 96 well plates in 100 µL culture medium. Cells were then treated with 1µM concentration of tested compounds, each dissolved in less than 0.1 % DMSO. After 72 h, cell growth was measured using the CellTiter 96® Aqueous One Solution Cell Proliferation Assay (Promega, Madison/WI, USA), in accordance with the manufacturer's instructions. Results are expressed as percentage proliferation compared to control cells.

Measurement of NF-kB transcriptional activity (HEK-Blue™ Detection). The tested compounds were dissolved in DMSO and further diluted in detection medium to a desired final concentration, so that the final concentration of DMSO did not exceed 0.1%. For screening for potential NOD1 inhibitors, HEK-Blue™-*h*NOD1 cells (5x10^5 cells/mL) were assayed in triplicate for NF-kB transcriptional activity after treatment with 10 µM compounds for 30 min,

followed by the addition of 100 ng/mL C12-iE-DAP and subsequent incubation for 18 h. For the selectivity, compounds were assayed under the same conditions with HEK-Blue™-*h*NOD2 cells (5x10^5 cells/mL) and 100 ng/mL MDP. For the specificity, compounds were assayed under the same conditions with HEK-Blue™-*h*NOD1 cells but C12-iE-DAP is replaced by TNFα (2.5 ng/mL). SEAP activity was determined spectrophotometrically as absorbance at 620 nm on a Clariostar Plus microplate reader (BMG Labtech). The percent inhibition at a specified concentration is determined or IC_{50} values are calculated based on a dose range of inhibitor concentrations using nonlinear regression in GraphPad Prism software. For THP1-Blue™ NF-kB cells, 1x10^6 cells were assayed in triplicate for NF-kB transcriptional activity after treatment with 10 µM compounds for 30 min, followed by the addition of 100 ng/mL C12-iE-DAP and subsequent incubation for 18 h. After induction, 2µL of QUANTI-Blue™ solution (InvivoGen) per well are dispensed and incubated at 37°C for 5-6 h, followed by absorbance measurement at 620 nm. IC_{50} values were calculated as described for HEK-Blue™ assay.

ADP-Glo™ In Vitro Kinase Assay. Recombinant RIPK2 protein (10 ng per reaction), KDR (1.5 ng per reaction) or EGFR (4 ng per reaction) was diluted in the reaction buffer consisting of 40 mM Tris (pH 7.5); 20mM $MgCl_2$; 0.1 mg/mL BSA; 50 µM DTT and 2mM $MnCl_2$ for EGFR. Diluted protein is added to low volume white 384 well plates (2 µL/well). Inhibitors are diluted in reaction buffer (final 25% DMSO), 1 µL is added to each well and incubated 10 min at room temperature. Reactions are initiated by the addition of 50 µM ATP and 1 µg/µL MBP protein for RIPK2, 0.2 µg/µL PGT for KDR or 5 µM ATP and 0.2 µg/µL PGT for EGFR in the reaction buffer. Plates are sealed with plastic coverslips and incubated at room temperature for 1 h. Reactions are stopped by the addition of 5 µL of ADP-Glo™ reagent (Promega) and ADP generation reaction is performed for 40 min at room temperature. Luminescence signal is generated by the addition of 10 µL of Kinase detection reagent (Promega) for 30 min at room temperature. Luminescence signals are determined using Clariostar Plus (BMG Labtech). The percent inhibition at a specified concentration is determined or IC_{50} values are calculated based on a dose range of inhibitor concentrations using nonlinear regression in GraphPad Prism software.

C12-iE-DAP-Stimulated IL-8 HTRF Assay. Tested compounds were prepared in DMSO and further diluted in culture medium to a desired final concentration and 5 µL was dispensed to individual wells of a 24 well plate. HEK-Blue™-*h*NOD1 cells (Invivogen) were prepared at 1×10^6 cells/mL in culture medium. Cell solution was dispensed at a volume of 500 µL/well in

24 well plate. Plate were incubated 1h. C12-iE-DAP (Invivogen) was prepared to 1 mg/mL stock solution in endotoxin free water. Stock C12-iE-DAP was further diluted in culture medium to 1x10^5 ng/mL and 5 µL was added to each well. Cell plates were placed in a 37 °C, 5% CO_2 incubator for 22 h. Following incubation, cell free supernatants obtained by centrifugation at 3000 rpm for 5 min and stored at -80 °C until measurement. IL-8 production was assessed by HTRF human IL-8 kit (Cisbio) according to the manufacturer's instructions. Fluorescence was read on a Clariostar Plus (BMG Labtech). Test compounds inhibition was expressed as percent inhibition.

Protein expression and purification. The cloning of the human RIPK2 construct encoding residues 1-317 is described in Lethier *et al*.[48] Protein was expressed in Sf21 insect cells and purified as described previously.[36] Briefly, cells were re-suspended in lysis buffer (20 mM Tris pH 7.5, 300 mM NaCl, 50 mM NDSB, 5% glycerol, 0.5 mM TCEP) containing a protease inhibitor cocktail (Complete, Roche) and lysed by sonication. After centrifugation at 48000×g for 30 min at 4°C, the supernatant solution was purified by amylose-affinity chromatography. After overnight cleavage with Tobacco Etch Virus (TEV) protease and dialysis against buffer A (20 mM Tris pH 7.5, 50 mM NaCl, 50 mM NDSB, 5% glycerol and 0.5 mM TCEP), the protein was further purified by anion exchange chromatography with a 0 to 1 M NaCl gradient. To remove TCEP and reduce the NaCl concentration to 150 mM, the sample was applied to a PD-10 column equilibrated in buffer B (20 mM Tris pH8, 150 mM NaCl, 25 mM NDSB, 2% glycerol). At the end of the purification, aliquots of protein at ~1 mg/ml concentration were flash-frozen in liquid nitrogen and stored at -80°C degrees.

Sample preparation and crystallization. Compound **37**, in powder form was solubilized in DMSO at 5 mM concentration. The RIPK2-compound **37** mixture was prepared as follows. One aliquot of protein at 1.14 mg/ml was thawed and mixed with 50 µM inhibitor and kept on ice for 10 minutes. The complex was than concentrated to 3.8 mg/ml. Crystallization conditions were established by trials with several commercial screens at the EMBL High Throughput Crystallization Laboratory (Grenoble, France) using a Cartesian robot. Crystals of RIPK2-compound **37** were obtained using the sitting drop method in CrystalDirect plates[49] from solutions containing 3.8 mg/ml of protein-inhibitor complex equilibrated against 0.1 M citric acid and 0.8 M sodium formate at pH 5. Crystals were harvested automatically using the CrystalDirect harvester[49] and cryo-cooled in liquid nitrogen.

Data Collection and structure solution. Diffraction data were collected automatically on the ID30-A1 (MASSIF) beamline at the ESRF.[50] Data were processed with autoPROC.[51] The structure was solved by molecular replacement using PHASER[52] using a previous RIPK2 structure as search model. The refinement restraints for the ligand were obtained using the AceDRG[53] from the CCP4i suite[54] using the compound SMILES. Refinement was carried out using REFMAC5[55] with manual rebuilding with COOT[56]. The model was validated using MolProbity[57] and structure figures were produced with Pymol (The PyMOL Molecular Graphics System, Version 3.0 Schrödinger, LLC.) and LigPlot+ (Laskowski & Swindells, 2011). Data collection and refinement statistics are given in Table 1 (Supporting informations).

Chemistry. 4-Chloro-6,7-dimethoxyquinazoline **1**, 4-chloro-6,7-bis(2-methoxyethoxy)-quinazoline **2** and 4-chloro-6,7,8-trimethoxyquinazoline **3** were purchased from Alfa Aesar. All commercial reagents and solvents were used without further purification. All reactions were monitored by analytical thin-layer chromatography (TLC) on 0.2 mm, Polygram SIL G/UV254 plates (Macherey-Nagel); compounds were visualized by UV (254 and 366 nm). Flash chromatography (FC) was performed with silica gel Kieselgel Si 60 0,015-0,040 mm (Macherey-Nagel). Melting points (Mp) were determined with a Büchi 535 capillary melting point apparatus and remain uncorrected. The structures of each compound were supported by IR (neat, FT- BrückerAlpha instrument). ^{1}H and ^{13}C NMR spectra were obtained using a Bruker® 300 MHz spectrometer, chemical shifts (δ) are expressed in ppm relative to tetramethylsilane (TMS) used as an internal, J values are in hertz, and the splitting patterns are designated as follows: s, singlet; d, doublet; t, triplet; q, quadruplet; quint, quintet; sex, sextuplet; m, multiplet. All compounds were analyzed by a UPLC system, an Acquity I-Class (Waters). Mass spectrometry was performed using a Xevo TQD (Waters Corporation) mass spectrometer. The detection of analytes was achieved by electrospray ionization (ESI) in the positive mode with the appropriate MRM transition. The LC-MS/MS instrument was controlled by MassLynx software (Waters). The purity of all compounds was determined by HPLC using a Chromazing column and a Waters 600 pump chromatograph equipped with a Waters 2487 dual absorption wavelength UV detector (λ = 254 nm and 366 nm). Retention time was obtained with flow rates of 1 mL/min. The acquisition time is 20 min. The mobile phase consisted of 0.8% formic acid in acetonitrile (80%) and water (20%).

General procedure for preparation of compounds 4-31

Method a

To a solution of 4-chloro-6,7-dimethoxyquinazoline **1** or 4-chloro-6,7-bis(2-methoxyethoxy)-quinazoline **2** (0.45 mmol) in isopropyl alcohol (4 mL) was added the corresponding aniline (0.54 mmol, 1.2 equiv.). The mixture was refluxed for 4-16 h and cooled to room temperature. The formed precipitate was isolated by filtration and washed with diethyl ether.

Method b

To a solution of 4-chloro-6,7-dimethoxyquinazoline **1** or 4-chloro-6,7,8-trimethoxyquinazoline **2** (0.45 mmol) in dry DMF (4 mL) were added the corresponding aniline (0.90 mmol, 2 equiv.) and 60% sodium hydride (1.35 mmol, 3 equiv.). The mixture was heated for 30 min at 50°C. Then, the mixture was cooled to room temperature and the solvent was removed under reduced pressure.

N-(2,4-dichloro-5-methoxyphenyl)-6,7-dimethoxyquinazolin-4-amine (4)

Compound **4** was synthesized using method b and purified on silica gel TLC glass plates eluting with CH_2Cl_2/MeOH (9/1) to give after crystallization from isopropyl alcohol, a beige solid. Mp = 224°C. Yield = 42%. IR (υ, cm^{-1}): 1077 (C-Cl). ^{1}H-NMR (DMSO, 300 MHz) δ ppm: 3.87 (s, 3H, OCH_3), 3.94 (s, 6H, $2OCH_3$), 7.18 (s, 1H, ArH), 7.34 (s, 1H, ArH), 7.70 (s, 1H, ArH), 7.81 (s, 1H, ArH), 8.31 (s, 1H, ArH), 9.61 (s, 1H, NH). ^{13}C NMR (DMSO, 75 MHz) δ ppm: 159.8 (C), 156.6 (C), 154.6 (C), 150.8 (C), 149.5 (CH), 136.8 (C), 134.8 (C), 130.4 (CH), 123.1 (C), 121.5 (C), 114.2 (CH), 107.3 (C), 103.9 (CH), 100.6 (CH), 57.4 (CH_3), 57.3 (CH_3), 57.0 (CH_3). LC-MS (ESI^+) *m/z* 380 $(M+H)^+$.

N-(2,4-dichlorophenyl)-6,7-dimethoxyquinazolin-4-amine hydrochloride (5)

Compound **5** was synthesized using method a and after crystallization from ethanol, was isolated as a white solid. Mp = 249°C. Yield = 17%. IR (υ, cm^{-1}): 2622 (NH^+), 1077 (C-Cl).

^{1}H-NMR (DMSO, 300 MHz) δ ppm: 4.01 (s, 6H, 2OCH$_3$), 7.42 (s, 1H, ArH), 7.61 (s, 2H, ArH), 7.87 (s, 1H, ArH), 8.34 (s, 1H, ArH), 8.80 (s, 1H, ArH), 11.74 (s, 1H, NH). ^{13}C NMR (DMSO, 75 MHz) δ ppm: 159.7 (C), 157.1 (C), 150.9 (C), 149.5 (CH), 136.4 (C), 134.0 (C), 133.3 (C), 132.8 (C), 131.5 (CH), 129.9 (CH), 128.6 (CH), 107.4 (CH), 104.3 (CH), 100.3 (CH), 57.3 (CH$_3$), 57.0 (CH$_3$). LC-MS (ESI$^+$) *m/z* 350 (M+H)$^+$.

N-(4-chloro-3-methoxyphenyl)-6,7-dimethoxyquinazolin-4-amine hydrochloride (6)

Compound **6** was synthesized using method a and after crystallization from methanol, was isolated as a beige solid. Mp > 250°C. Yield = 45%. IR (υ, cm^{-1}): 2617 (NH$^+$), 1062 (C-Cl). ^{1}H-NMR (DMSO, 300 MHz) δ ppm: 3.88 (s, 3H, OCH$_3$), 3.99 (s, 3H, OCH$_3$), 4.04 (s, 3H, OCH$_3$), 7.39 (s, 1H, ArH), 7.39-7.43 (dd, 1H, ArH, *J* = 2.2 Hz and *J* = 8.5 Hz), 7.49-7.52 (d, 1H, ArH, *J* = 8.5 Hz), 7.64-7.65 (d, 1H, ArH, *J* = 2.2 Hz), 8.43 (s, 1H, ArH), 11.60 (s, 1H, ArH), 11.99 (s, 1H, NH). ^{13}C NMR (DMSO, 75 MHz) δ ppm: 158.6 (C), 156.8 (C), 154.8 (C), 150.7 (CH), 149.0 (CH), 137.6 (C), 136.1 (C), 130.0 (CH), 118.7 (C), 118.1 (C), 110.0 (CH), 107.8 (C), 104.5 (CH), 100.2 (CH), 57.6 (CH$_3$), 56.9 (CH$_3$), 56.7 (CH$_3$). LC-MS (ESI$^+$) *m/z* 346 (M+H)$^+$.

N-(2-chloro-5-methoxyphenyl)-6,7-dimethoxyquinazolin-4-amine hydrochloride (7)

Compound **7** was synthesized using method a and after crystallization from ethanol, was isolated as a beige solid. Mp > 250°C. Yield = 39%. IR (υ, cm^{-1}): 2575 (NH$^+$), 1085 (C-Cl). ^{1}H-NMR (DMSO, 300 MHz) δ ppm: 3.80 (s, 3H, OCH$_3$), 4.02 (s, 6H, 2OCH$_3$), 7.04-7.08 (d, 1H, ArH, *J* = 7.8 Hz), 7.17 (s, 1H, ArH), 7.45 (s, 1H, ArH), 7.54-7.58 (d, 1H, ArH, *J* = 8.7 Hz), 8.36 (s, 1H, ArH), 8.80 (s, 1H, ArH), 11.75 (s, 1H, NH). ^{13}C NMR (DMSO, 75 MHz) δ ppm: 159.7 (C), 159.1 (C), 157.0(C), 150.8 (CH), 149.2 (CH), 136.1 (C), 135.4 (C), 130.8 (CH), 122.8 (C), 115.7 (C), 115.4 (C), 107.2 (CH), 104.4 (CH), 100.2 (CH), 57.4 (CH$_3$), 57.0 (CH$_3$), 52.3 (CH$_3$). LC-MS (ESI$^+$) *m/z* 346 (M+H)$^+$.

N-(4-chlorophenyl)-6,7-dimethoxyquinazolin-4-amine hydrochloride (8)

Compound **8** was synthesized using method a and was isolated as a white solid. Mp > 250°C. Yield = 81%. IR (υ, cm^{-1}): 2626 (NH^+), 1228 (C-O-C), 1088 (C-Cl). ^{1}H-NMR (DMSO, 300 MHz) δ ppm: 3.99 (s, 3H, OCH_3), 4.02 (s, 3H, OCH_3), 7.35 (s, 1H, ArH), 7.53-7.56 (d, 2H, ArH, *J* = 8.7 Hz), 7.75-7.78 (d, 2H, ArH, *J* = 8.7 Hz), 8.34 (s, 1H, ArH), 8.84 (s, 1H, ArH), 11.45 (s, 1H, NH). ^{13}C NMR (DMSO, 75 MHz) δ ppm: 158.6 (C), 156.8 (C), 150.7 (C), 149.2 (CH), 136.5 (C), 136.3 (C), 131.6 (C), 129.1 (2CH), 126.8 (2CH), 107.9 (C), 104.5 (CH), 100.4 (CH), 57.5 (CH_3), 56.9 (CH_3). LC-MS (ESI) *m/z* 316 $(M+H)^+$.

N-(2-chlorophenyl)-6,7-dimethoxyquinazolin-4-amine hydrochloride (9)

Compound **9** was synthesized using method a and after crystallization from ethanol, was isolated as a yellow solid. Mp = 249°C. Yield = 20%. IR (υ, cm^{-1}): 2515 (NH^+), 1074 (C-Cl). ^{1}H-NMR (DMSO, 300 MHz) δ ppm: 4.01 (s, 6H, $2OCH_3$), 7.42 (s, 1H, ArH), 7.49-7.59 (m, 3H, ArH), 7.62-7.67 (dd, 1H, ArH, *J* = 1.9 Hz and *J* = 7.4 Hz), 8.33 (s, 1H, ArH), 8.78 (s, 1H, ArH), 11.67 (s, 1H, NH). ^{13}C NMR (DMSO, 75 MHz) δ ppm: 159.8 (C), 157.0 (C), 150.8 (C), 149.3 (CH), 136.1 (C), 134.7 (C), 131.5 (C), 130.5 (CH), 130.3 (CH), 129.8 (CH), 128.5 (CH), 107.2 (C), 104.3 (CH), 100.3 (CH), 57.3 (CH_3), 57.0 (CH_3). LC-MS (ESI^+) *m/z* 316 $(M+H)^+$.

N-(3,4-dichlorophenyl)-6,7-dimethoxyquinazolin-4-amine hydrochloride (10)

Compound **10** was synthesized using method a and isolated as a beige solid. Mp > 250°C. Yield = 88%. IR (υ, cm^{-1}): 2496 (NH^+), 1071 (C-Cl). ^{1}H-NMR (DMSO, 300 MHz) δ ppm: 3.97 (s, 3H, OCH_3), 4.00 (s, 3H, OCH_3), 7.26 (s, 1H, ArH), 7.66-7.69 (d, 1H, ArH, *J* = 9.1 Hz), 7.87-7.91 (dd, 1H, ArH, *J* = 2.6 Hz and *J* = 8.7 Hz), 8.03 (s, 1H, ArH), 8.22-8.24 (d, 1H, ArH, *J* = 2.0 Hz), 8.64 (s, 1H, ArH), 10.32 (s, 1H, NH). ^{13}C NMR (DMSO, 75 MHz) δ ppm: 157.1 (C), 155.7 (C), 151.7 (CH), 150.1 (C), 143.7 (C), 139.5 (C), 131.2 (C) 130.9 (CH), 126.0 (C), 124.4

(CH), 123.1 (CH), 108.6 (C), 105.2 (CH), 103.0 (CH), 57.1 (CH_3), 56.6 (CH_3). LC-MS (ESI^+) *m/z* 350 $(M+H)^+$.

N-(3-chlorophenyl)-6,7-dimethoxyquinazolin-4-amine hydrochloride (11)

Compound **11** was synthesized using method a and isolated as a white solid. Mp > 250°C. Yield = 85%. IR (υ, cm^{-1}): 2466 (NH^+), 1085 (C-Cl). ^{1}H-NMR (DMSO, 300 MHz) δ ppm: 4.01 (s, 3H, OCH_3), 4.03 (s, 3H, OCH_3), 7.32-7.35 (m, 2H, ArH), 7.51-7,55 (m, 1H, ArH), 7.73-7.75 (d, 1H, ArH, *J* = 7.8 Hz), 7.88-7.89 (m, 1H, ArH), 8.41 (s, 1H, ArH), 8.87 (s, 1H, ArH), 11.61 (s, 1H, NH). ^{13}C NMR (DMSO, 75 MHz) δ ppm: 158.6 (C), 157.0 (C), 150.8 (C), 149.4 (CH), 139.1 (C), 136.7 (C), 133.3 (C), 130.8 (C), 129.3 (CH), 126.3 (CH), 124.7 (CH), 123.5 (CH), 107.9 (C), 104.4 (CH), 100.5 (CH), 57.5 (CH_3), 57.0 (CH_3). LC-MS (ESI^+) *m/z* 316 $(M+H)^+$.

N-(2,5-dibromophenyl)-6,7-dimethoxyquinazolin-4-amine hydrochloride (12)

Compound **12** was synthesized using method a and after crystallization from ethanol, was isolated as a white solid. Mp > 250°C. Yield = 60%. IR (υ, cm^{-1}): 2465 (NH^+), 1059 (C-Br). ^{1}H-NMR (DMSO, 300 MHz) δ ppm: 4.01 (s, 6H, $2OCH_3$), 7.39 (s, 1H, ArH), 7.58-7.61 (dd, 1H, ArH, *J* = 2.4 Hz and *J* = 8.4 Hz), 7.78-7.81 (d, 1H, ArH, *J* = 8.7 Hz), 7.84-7.85 (s, 1H, ArH, *J* = 2.3 Hz), 8.29 (s, 1H, ArH), 8.82 (s, 1H, ArH), 11.69 (s, 1H, NH). ^{13}C NMR (DMSO, 75 MHz) δ ppm: 159.7 (C), 157.1 (C), 150.9 (C), 149.4 (CH), 138.0 (C), 136.4 (C), 135.2 (CH), 133.0 (CH), 132.8 (CH), 121.7 (C), 121.1 (C), 107.3 (C), 104.1 (CH), 100.4 (CH), 57.3 (CH_33), 57.0 (CH_3), 52.3 (CH_3). LC-MS (ESI^+) *m/z* 346 $(M+H)^+$.

N-(3-chloro-4-fluorophenyl)-6,7-dimethoxyquinazolin-4-amine hydrochloride (13)

Compound **13** was synthesized using method a and was isolated as a white solid. Mp = 153°C. Yield = 56%. IR (υ, cm^{-1}): 2467 (NH^+), 1221 (C-F), 1075 (C-Cl). ^{1}H-NMR (DMSO, 300 MHz) δ ppm: 4.01 (s, 3H, OCH_3), 4.03 (s, 3H, OCH_3), 7.34 (s, 1H, ArH), 7.54-7.58 (m, 1H, ArH), 7.73-7.78 (m, 1H, ArH), 8.02-8.06 (dd, 1H, ArH, *J* = 2.5 Hz and *J* = 7.1 Hz), 8.32 (s, 1H, ArH),

8.89 (s, 1H, ArH), 11.45 (s, 1H, NH). ^{13}C NMR (DMSO, 75 MHz) δ ppm: 158.7 (C), 156.8 (C), 150.7 (CH), 149.6 (C), 141.2 (C), 134.7 (C), 130.7 (C), 127.1 (CH), 125.6 (CH), 117.5 (CH), 117.2 (CH), 107.8 (C), 104.2 (CH), 100.7 (C), 57.4 (CH3), 56.9 (CH3). LC-MS (ESI) *m/z* 334 $(M+H)^+$.

N-(4-bromo-6-fluorophenyl)-6,7-dimethoxyquinazoin-4-amine hydrochloride (14)

Compound **14** was synthesized using method a and after crystallization from ethanol, was isolated as a white solid. Mp = 215°C. Yield = 46%. IR (υ, cm^{-1}): 2716 (NH^+), 1240 (C-F), 1063 (C-Br). ^{1}H-NMR (DMSO, 300 MHz) δ ppm: 4.00 (s, 6H, $2OCH_3$), 7.39 (s, 1H, ArH), 7.52-7.59 (m, 2H, ArH), 7.77-7.83 (d, 1H, ArH, *J* = 2.1 Hz), 8.31-8.37 (d, 1H, ArH, *J* = 8.3 Hz), 8.82 (s, 1H, ArH), 12.50 (s, 1H, NH). ^{13}C NMR (DMSO, 75 MHz) δ ppm: 159.0 (C), 157.1 (C), 150.8 (C), 149.3 (CH), 136.3 (C), 130.7 (C), 128.4 (C), 124.7 (C), 120.8 (CH), 120.6 (CH), 120.0 (CH), 107.5 (C), 104.4 (CH), 400.3 (CH), 57.5 (CH_3), 57.4 (CH_3), 57.0 (CH_3). LC-MS (ESI^+) *m/z* 378 $(M+H)^+$.

N-(4-bromo-2-fluoro-5-methoxyphenyl)-6,7-dimethoxyquinazolin-4-amine hydrochloride (15)

Compound **15** was synthesized using method a and after crystallization from ethanol, was isolated as a grey solid. Mp > 250°C. Yield = 57%. IR (υ, cm^{-1}): 2631 (NH^+), 1226 (C-F), 1069 (C-Br). ^{1}H-NMR (DMSO, 300 MHz) δ ppm: 3.86 (s, 3H, OCH_3), 4.02 (s, 6H, $2OCH_3$), 7.34 (s, 1H, ArH), 7.36-7.37 (d, 1H, ArH, *J* = 7.0 Hz), 7.84-7.85 (d, 1H, ArH, *J* = 9.5 Hz), 8.27 (s, 1H, ArH), 8.83 (s, 1H, ArH), 11.51 (s, 1H, NH). ^{13}C NMR (DMSO, 75 MHz) δ ppm: 159.4 (C), 157.1 (C), 152.8 (C), 152.6 (C), 150.8 (CH), 136.8 (C), 124.9 (C), 124.7 (CH), 121.1 (C), 120.7 (C), 112.5 (CH), 107.6 (C), 104.1 (CH), 100.5 (CH), 57.5 (CH_3), 57.3 (CH_3), 57.0 (CH_3). LC-MS (ESI^+) *m/z* 410 $(M+H)^+$.

2,4-dichloro-5-((6,7-dimethoxyquinazolin-4-yl)amino)phenol (16)

Compound **16** was synthesized using method a and was purified on silica gel TLC glass plates eluting with CH_2Cl_2/MeOH (9/1) to give a white solid. Mp > 250 °C. Yield = 17%. IR (υ, cm^{-1}): 3551 (OH), 1081 (C-Cl). ^{1}H-NMR (DMSO, 300 MHz) δ ppm: 3.94 (s, 6H, 2OCH_3), 7.17 (s, 1H, ArH), 7.20 (s, 1H, ArH), 7.60 (s, 1H, ArH), 7.81 (s, 1H, ArH), 8.35 (s, 1H, ArH), 9.46 (s, 1H, NH), 10.61 (s, 1H, OH). ^{13}C NMR (DMSO, 75 MHz) δ ppm: 157.7 (C), 154.8 (C), 153.5 (C), 152.8 (C), 149.4 (CH), 147.4 (C), 136.2 (C), 130.1 (CH), 121.1 (C), 118.2 (C), 117.0 (CH), 109.0 (C), 107.5 (CH), 102.3 (CH), 57.6 (CH_3), 57.3 (CH_3). LC-MS (ESI^+) *m/z* 366 $(M+H)^+$.

2-chloro-5-((6,7-dimethoxyquinazolin-4-yl)amino)phenol hydrochloride (17)

Compound **17** was synthesized using method a and after crystallization from methanol, was isolated as a yellow solid. Mp > 250°C. Yield = 80%. IR (υ, cm^{-1}): 3169 (OH), 2784 (NH^+). ^{1}H-NMR (DMSO, 300 MHz) δ ppm: 4.00 (s, 3H, OCH_3), 4.02 (s, 3H, OCH_3), 7.16-7.20 (dd, 1H, ArH, *J* = 2.4 Hz and *J* = 8.6 Hz), 7.39-7.43 (m, 3H, ArH), 8.36 (s, 1H, ArH), 8.84 (s,1H, ArH), 10.59 (s, 1H, OH), 11.41 (s, 1H, NH). ^{13}C NMR (DMSO, 75 MHz) δ ppm: 158.5 (C), 156.7 (C), 153.6 (C), 150.6 (C), 149.3 (CH), 137.0 (C), 136.6 (C), 130.0 (CH), 117.6 (C), 116.9 (CH), 113.3 (CH), 107.8 (C), 104.3 (CH), 100.6 (CH), 57.3 (CH_3), 56.9 (CH_3). LC-MS (ESI^+) *m/z* 332 $(M+H)^+$.

3-((6,7-dimethoxyquinazolin-4-yl)amino)phenol hydrochloride (18)

Compound **18** was synthesized using method a and was isolated as a yellow solid. Mp = 153°C. Yield = 91%. IR (υ, cm^{-1}): 3198 (OH), 2835 (NH). ^{1}H-NMR (DMSO, 300 MHz) δ ppm: 4.00 (s, 6H, 2OCH_3), 6.73-6.76 (m, 1H, ArH), 7.09-7.12 (m, 2H, ArH), 7.25-7.27 (m, 1H, ArH), 7.36 (s, 1H, ArH), 8.27 (s, 1H, ArH), 8.82 (s, 1H, ArH), 9.74 (s,1H, NH), 11.19 (s, 1H, OH). ^{13}C NMR (DMSO, 75 MHz) δ ppm: 158.6 (C), 158.2 (C), 156.7 (CH), 150.7 (C), 149.2 (CH), 138.2 (C), 136.0 (C), 129.9 (C), 115.9 (CH), 114.0 (CH), 112.4 (CH), 107.7 (C), 104.4 (CH), 100.4 (CH), 57.3 (CH_3), 56.9 (CH_3). LC-MS (ESI^+) *m/z* 298 $(M+H)^+$.

2-bromo-5-((6,7-dimethoxyquinazolin-4-yl)amino)phenol (19)

Compound **19** was synthesized using method a and after crystallization from acetonitrile, was isolated as an orange solid. Mp > 250 °C. Yield 50%. IR (υ, cm^{-1}): 3423 (OH), 2388 (NH), 773 (C-Br). ^{1}H NMR (DMSO, 300 MHz) δ ppm: 3.94 (s, 6H, $2OCH_3$), 7.06 (dd, 1H, *J* = 8.2 Hz, *J* = 2.3 Hz, ArH), 7.12 (d, 1H, *J* = 2.3 Hz, ArH), 7.18 (s, 1H, ArH), 7.41 (d, 1H, *J* = 8.2 Hz, ArH), 7.85 (s, 1H, ArH), 8.37 (s, 1H, ArH), 9.31 (s, 1H, NH), 10.32 (s, 1H, OH). ^{13}C NMR (DMSO, 75 MHz) δ ppm: 157.6 (C), 154.6 (C), 153.3 (C), 153.2 (CH), 149.2 (C), 147.1 (C), 129.2 (C), 126.7 (CH), 122.1 (C), 119.5 (CH), 118.1 (CH), 109.2 (CH), 107.5 (C), 102.6 (CH), 56.6 (CH_3), 56.2 (CH_3). LC-MS (ESI^+) m/z 378 ($M+H^+$).

5-((6,7-dimethoxyquinazolin-4-yl)amino)-2-fluorophenol (20)

Compound **20** was synthesized using method a and after crystallization from acetonitrile, was isolated as a white solid. Mp > 250°C. Yield 85%. IR (υ, cm^{-1}): 2913 (OH), 1114 (C-F). ^{1}H NMR (DMSO, 300 MHz) δ ppm: 3.93 (s, 3H, OCH_3), 3.95 (s, 3H, OCH_3), 7.15-7.12 (d, 1H, *J* = 8.4 Hz, ArH), 7.18 (s, 1H, ArH), 7.51-7.48 (d, 1H, *J* = 8.7 Hz, ArH), 7.82 (s, 1H, ArH), 8.44 (s, 1H, ArH), 9.38 (s, 1H, ArH). ^{13}C NMR (DMSO, 75 MHz) δ ppm: 156.8 (C), 154.6 (C), 153.3 (CH), 149.5-146.3 (d, J_{CF} = 237 Hz, C), 149.2 (C), 147.3 (C), 144.9-144.7 (d, J_{CF} = 14.2 Hz, C), 136.2-136.1 (d, J_{CF} = 2.6 Hz, C), 116.0-115.7 (d, J_{CF} = 18.3 Hz, CH), 113.8-113.7 (d, J_{CF} = 6.3 Hz, CH), 112.8-112.7 (d, J_{CF} = 2.3 Hz, CH), 109.2 (CH), 107.6 (C), 102.3 (CH), 56.6 (CH_3), 56.2 (CH_3), LC-MS (ESI^+) *m/z* 316 ($M+H^+$).

4-chloro-N-(6,7-dimethoxyquinazolin-4-yl)benzene-1,3-diamine (21)

Compound **21** was synthesized using method a and after crystallization from acetonitrile, was isolated as a beige solid. Mp = 243°C. Yield 33%. IR (υ, cm^{-1}): 2688 (NH_2), 618 (C-Cl). ^{1}H NMR (DMSO, 300 MHz) δ ppm: 3.98 (s, 3H, OCH_3), 4.02 (s, 3H, OCH_3), 6.90-6.86 (dd, 1H, *J* = 8.3 Hz, *J* = 2.3 Hz, ArH), 7.12-7.11 (d, 1H, *J* =2.3 Hz, ArH), 7.27-7.24 (d, 1H, *J* = 8.3 Hz,

ArH), 7.48 (s, 1H, ArH), 8.45 (s, 1H, ArH), 8.77 (s, 1H, ArH), 11.46 (s, 1H, NH). ^{13}C NMR (DMSO, 75 MHz) δ ppm: 157.9 (C), 156.2 (C), 150.0 (C), 148.5 (C), 144.6 (CH), 135.7 (C), 134.8 (C), 128.9 (CH), 114.8 (C), 114.1 (CH), 113.4 (CH), 111.2 (CH), 106.7 (C), 103.2 (CH), 56.4 (CH_3), 56.3 (CH_3). LC-MS (ESI^+) m/z 331 ($M+H^+$).

N-(6,7-dimethoxyquinazolin-4-yl)benzene-1,3-diamine (22)

Compound **22** was synthesized using method a and purified on silica gel TLC glass plates eluting with CH_2Cl_2/MeOH (9/1) to give a grey solid. Mp > 250°C. Yield = 64%. IR (υ, cm^{-1}): 3315 (NH_2), 2837 (NH). ^{1}H-NMR (DMSO, 300 MHz) δ ppm: 3.99 (s, 3H, OCH_3), 4.00 (s, 3H, OCH_3), 6.60-6.63 (d, 1H, ArH, *J* = 7.9 Hz), 6.92-6.94 (d, 1H, ArH, *J* = 8.1 Hz), 6.98 (s, 1H, ArH), 7.14-7.19 (m, 1H, ArH), 7.34 (s, 1H, ArH), 8.23 (s, 1H, ArH), 8.76 (s, 1H, ArH), 10.97 (s, 1H, NH). ^{13}C NMR (DMSO, 75 MHz) δ ppm: 158.2 (C), 156.5 (C), 150.5 (C), 149.4 (CH), 147.6 (C), 137.8 (C), 136.9 (C), 129.7 (CH), 113.9 (CH), 113.5 (CH), 111.3 (CH), 107.6 (C), 103.7 (CH), 101.0 (CH), 57.0 (CH_3), 56.9 (CH_3). LC-MS (ESI^+) *m/z* 297 $(M+H)^+$.

6,7-dimethoxy-N-phenylquinazolin-4-amine hydrochloride (23)

Compound **23** was synthesized using method a was isolated as a white solid. Mp = 136 °C. Yield = 55%. IR (υ, cm^{-1}): 2667 (NH^+). ^{1}H-NMR (DMSO, 300 MHz) δ ppm: 4.00 (s, 3H, OCH_3), 4.03 (s, 3H, OCH_3), 7.31-7.33 (m, 1H, ArH), 7.40 (s, 1H, ArH), 7.46-7.52 (m, 2H, ArH), 7.69-7.72 (m, 2H, ArH), 8.41 (s, 1H, ArH), 8.82 (s, 1H, ArH), 11.55 (s, 1H, NH). ^{13}C NMR (DMSO, 75 MHz) δ ppm: 158.6 (C), 156.7 (C), 150.6 (C), 149.1 (CH), 137.3 (C), 135.9 (C), 129.2 (2CH), 126.8 (CH), 125.4 (2CH), 107.7 (C), 104.4 (CH), 100.4 (CH), 57.5 (CH_3), 56.9 (CH_3). LC-MS (ESI^+) *m/z* 282 $(M+H)^+$.

N2-(6,7-dimethoxyquinazolin-4-yl)pyridine-2,4-diamine (24)

Compound **24** was synthesized using method a and purified by flash chromatography eluting with CH_2Cl_2/MeOH (9/1) to give a beige solid. Mp > 250°C. Yield = 73%. IR (υ, cm^{-1}): 2599

(NH$^+$). ^{1}H-NMR (DMSO, 300 MHz) δ ppm: 3.88 (s, 3H, OCH_3), 4.06 (s, 3H, OCH_3), 6.06 (s, 1H, ArH), 6.41-6.44 (dd, 1H, ArH, *J* = 1.2 Hz and *J* = 7.3 Hz), 6.84 (s, 1H, ArH), 7.35 (s, 2H, ArH), 7.60 (s, 1H, ArH), 7.72-7.75 (d, 2H, ArH), 9.19 (s, 1H, NH). ^{13}C NMR (DMSO, 75 MHz) δ ppm: 158.7 (C), 156.8 (C), 153.8 (C), 152.0 (CH) 150.8 (C), 149.3 (CH), 136.2 (C), 135.9 (C), 131.7 (C), 123.3 (CH), 122.9 (CH), 119.4 (CH), 107.8 (C), 104.5 (CH), 100.4 (CH), 57.4 (CH_3), 56.8 (CH_3). LC-MS (ESI$^+$) *m/z* 339 (M+H)$^+$.

6,7-dimethoxy-N-(pyridin-4-yl)quinazolin-4-amine (25)

Compound **25** was synthesized using method a and after crystallization from ethanol, was isolated as a yellow solid. Mp = 243°C. Yield = 55%. IR (υ, cm^{-1}): 3230 (NH). ^{1}H-NMR (DMSO, 300 MHz) δ ppm: 3.95 (s, 3H, OCH_3), 4.06 (s, 3H, OCH_3), 7.31-7.33 (m, 3H, ArH), 7.60 (s, 1H, ArH), 8.64-8.66 (m, 2H, ArH), 9.15 (s, 1H, ArH), 9.17 (s, 1H, NH). ^{13}C NMR (DMSO, 75 MHz) δ ppm: 160.9 (C), 157.6 (C), 156.2 (C), 152.8 (CH), 152.0 (C), 151.5 (C), 142.5 (CH), 113.6 (2CH), 109.9 (CH), 107.5 (2CH), 101.4 (CH), 57.1 (CH_3), 56.7 (CH_3). LC-MS (ESI$^+$) *m/z* 283 (M+H)$^+$.

N-(4,5-dimethyl-1H-pyrazol-3-yl)-6,7-dimethoxyquinazolin-4-amine (26)

Compound **26** was synthesized using method a and purified on silica gel TLC glass plates eluting with CH_2Cl_2/MeOH (9/1) to give a yellow solid. Mp = 123 °C. Yield = 23%. IR (υ, cm^{-1}): 3184 (NH). ^{1}H-NMR (DMSO, 300 MHz) δ ppm: 1.76 (s, 3H, CH_3), 2.18 (s, 3H, CH_3), 3.92 (s, 3H, OCH_3), 3.94 (s, 3H, OCH_3), 7.16 (s, 1H, ArH), 7.85 (s, 1H, ArH), 8.31 (s, 1H, ArH), 9.50 (s, 1H, NH), 12.13 (s, 1H, NH). ^{13}C NMR (DMSO, 75 MHz) δ ppm: 159.6 (C), 156.8 (C), 150.7 (C), 149.1 (CH), 137.6 (C), 136.1 (C), 108.1 (C), 107.2 (C), 104.2 (CH), 100.3 (CH), 57.1 (CH_3), 56.9 (CH_3), 10.0 (CH_3), 8.2 (CH_3). LC-MS (ESI$^+$) *m/z* 300 (M+H)$^+$.

N-(6,7-dimethoxyquinazolin-4-yl)benzo[d]thiazol-5-amine hydrochloride (27)

Compound **27** was synthesized using method a and after crystallization from methanol, was isolated as a beige solid. Mp > 250°C. Yield = 73%. IR (υ, cm^{-1}): 2599 (NH^+). ^{1}H-NMR (DMSO, 300 MHz) δ ppm: 4.01 (s, 3H, OCH_3), 4.05 (s, 3H, OCH_3), 7.38 (s, 1H, ArH), 7.83-7.87 (dd, 1H, ArH, *J* = 2.0 Hz and *J* = 8.4 Hz), 8.25-8.28 (d, 1H, ArH, *J* = 8.4 Hz), 8.42-8.49 (m, 2H, ArH), 8.86 (s, 1H, ArH), 9.48 (s, 1H, ArH), 11.66 (s, 1H, NH). ^{13}C NMR (DMSO, 75 MHz) δ ppm: 158.7 (C), 156.8 (C), 153.8 (C), 152.0 (CH) 150.8 (C), 149.3 (CH), 136.2 (C), 135.9 (C), 131.7 (C), 123.3 (CH), 122.9 (CH), 119.4 (CH), 107.8 (C), 104.5 (CH), 100.4 (CH), 57.4 (CH_3), 56.8 (CH_3). LC-MS (ESI^+) *m/z* 339 $(M+H)^+$.

N-(5-fluoro-1H-indazol-3-yl)-6,7-dimethoxyquinazolin-4-amine (28)

Compounds **28** was synthesized using method a and purified by column chromatography on silica gel eluting with CH_2Cl_2/MeOH (9/1) to give a yellow solid. Mp > 250°C. Yield = 28%. IR (cm^{-1}: neat): 1220 (C-F). ^{1}H-NMR (DMSO) δ ppm: 4.01 (s, 6H, $2OCH_3$), 7.21 (s, 1H, ArH), 7.24-7.29 m, 2H, ArH), 7.53-7.58 (m, 1H, ArH), 7.97 (s, 1H, ArH), 8.34 (s, 1H, ArH), 10.16 (s, 1H, NH), 12.93 (s, 1H, NH). ^{13}C NMR (DMSO, 75Hz) δ ppm: 158.2 (C), 157.7 (C), 155.1 (CH), 154.8 (C), 153.5 (C), 149.3 (C), 147.3 (CH), 138.8 (C), 116.4 (C), 116.0 (CH), 112.6 (C), 112.4 (CH), 107.4 (CH), 106.3 (CH), 102.7 (CH), 56.6 (CH_3), 56.3 (CH_3). LC-MS (ESI^+) *m/z* 340 $(M+H)^+$.

1-(6,7-dimethoxyquinazolin-4-yl)-5-fluoro-1H-indazol-3-amine (29)

Compounds **29** was synthesized using method a and purified by column chromatography on silica gel eluting with CH_2Cl_2/MeOH (9/1) to give a beige solid. Mp > 250°C. Yield = 6%. IR (cm^{-1}: neat): 3191 (NH_2), 1220 (C-F). ^{1}H-NMR (DMSO) δ ppm: 3.98 (s, 6H, $2OCH_3$), 6.57 (s, 2H, NH_2), 7.31 (s, 1H, ArH), 7.44-7.51 (m, 1H, ArH), 7.74-78 (dd, 2H, ArH, *J* = 2.4 Hz and *J* = 8.4 Hz), 8.77-8.80 (m, 1H, ArH), 8.82 (s, 1H, ArH), 9.15 (s, 1H, NH). ^{13}C NMR (DMSO, 75Hz) δ ppm: 159.8 (C), 155.2 (CH), 154.2 (C), 152.9 (C) 152.2 (C), 150.6 (C), 149.1 (C),

138.2 (C), 119.6 (CH), 118.8 (CH), 117.5 (C), 110.8 (CH), 107.5 (CH), 107.2 (CH), 106.0 (CH), 56.4 (CH_3), 56.2(CH_3). LC-MS (ESI^+) *m/z* 340 $(M+H)^+$.

N-(2,4-dichloro-5-methoxyphenyl)-6,7-bis(2-methoxyethoxy)quinazolin-4-amine (30)

Compound **30** was synthesized using method b and was isolated as a grey solid. Mp = 184°C. Yield = 73%. IR (υ, cm^{-1}): 1125 (C-O-C), 1074 (C-Cl). ^{1}H-NMR (DMSO, 300 MHz) δ ppm: 3.36 (s, 3H, OCH_3), 3.38 (s, 3H, OCH_3), 3.74-3.80 (m, 4H,CH_2), 3.87 (s, 3H, OCH_3), 4.26-4.30 (m, 4H,CH_2), 7.22 (s, 1H, ArH), 7.38 (s, 1H, ArH), 7.71 (s, 1H, ArH), 7.87 (s, 1H, ArH), 8.35 (s, 1H, ArH), 9.60 (s, 1H, NH). ^{13}C NMR (DMSO, 75 MHz) δ ppm: 157.8 (C), 154.2 (C), 153.5 (CH), 148.5 (C), 147.3 (C), 136.8 (C), 130.2 (CH), 122.9 (C), 119.5 (C), 114.1 (CH), 109.1 (C), 108.5 (CH), 103.6 (CH), 70.6 (CH_2), 68.7 (CH_2), 68.5 (CH_2), 58.9 (CH_3), 58.8 (CH_3), 57.1 (CH_3). LC-MS (ESI^+) *m/z* 468 $(M+H)^+$.

N-(2,4-dichloro-5-methoxyphenyl)-6,7,8-trimethoxyquinazolin-4-amine (31)

Compound **34** was synthesized using method b and was isolated as a white solid. Mp = 177°C. Yield = 16%. IR (υ, cm^{-1}): 1129 (C-O-C), 1079 (C-Cl). ^{1}H-NMR (DMSO, 300 MHz) δ ppm: 3.87 (s, 3H, OCH_3), 3.92 (s, 3H, OCH_3), 3.97 (s, 3H, OCH_3), 4.01 (s, 3H, OCH_3), 7.34 (s, 1H, ArH), 7.70 (s, 1H, ArH), 7.72 (s, 1H, ArH), 8.38 (s, 1H, ArH), 9.74 (s, 1H, NH). ^{13}C NMR (DMSO, 75 MHz) δ ppm: 158.4 (C), 154.2 (C), 152.6 (C), 152.5 (CH), 147.4 (C), 146.7 (C), 141.5 (C), 136.6 (C), 130.2 (CH), 123.2 (C), 119.8 (C), 114.1 (CH), 111.5 (C), 98.5 (CH), 62.3 (CH_3), 61.4 (CH_3), 57.1 (CH_3), 56.8 (CH_3). LC-MS (ESI^+) *m/z* 410 $(M+H)^+$.

Methyl 4-(2-(diethylamino)ethoxy)-3-methoxybenzoate hydrochloride (32)

Potassium carbonate (0.44 mol, 4 equiv.) was added to a solution of methyl vanillate (0.11 mol) in acetone (300 mL) and was stirred for 5 min. 2-Diethylaminoethyl chloride hydrochloride (0.16 mol, 1.5 equiv.) was added and the mixture was refluxed for 16 h. The inorganic solid was filtered off and the filtrate was concentrated under vacuum. The oily residue was dissolved

in 2-propanol (10 mL) and 2-propanol saturated with HCl was added (15 mL). The resulting white precipitate was filtered, washed with diethyl ether, and dried under vacuum to afford **32**. Mp = 91°C. Yield = 76%. IR (υ, cm^{-1}): 2473 (NH^+), 1707 (C=O). ^1H NMR (DMSO, 300 MHz) δ ppm: 1.23-1.28 (m, 6H, $2NCH_2CH_3$), 3.21-3.23 (m, 4H, $2NCH_2CH_3$), 3.50-3.54 (t, 2H, NCH_2CH_2O, *J* = 4.6 Hz), 3.82 (s, 3H, OCH_3), 3.83 (s, 3H, OCH_3), 4.43-4.47 (t, 2H, NCH_2CH_2O, *J* = 4.6 Hz), 7.13-7.15 (d, 1H, ArH, *J* = 8.7 Hz), 7.48-7.49 (d, 1H, ArH, *J* = 2.1 Hz), 7.61-7.62 (dd, 1H, ArH, *J* = 8.7 Hz and *J* = 2.1 Hz), 10.53 (s, 1H, NH^+). LC/MS (ESI^+) *m/z* 282 $(M+H)^+$.

Methyl 4-(2-(diethylamino)ethoxy)-5-methoxy-2-nitrobenzoate hydrochloride (33)

A solution of tin (IV) chloride (28 mmol, 3 equiv.) and nitric fuming acid (28 mmol, 3 equiv.) in CH_2Cl_2 (20 mL) was added dropwise to a solution of **32** (9.40 mmol) in CH_2Cl_2 (150 mL) cooled at -70°C. After stirring for 8 h at -70°C and warming to room temperature, the residue was filtered off and dissolved in saturated potassium carbonate solution (100 mL). The aqueous solution was then extracted with ethyl acetate (3 × 70 mL), dried over magnesium sulfate, and concentrated under vacuum. The oily residue was dissolved in 2-propanol (3 mL), and 2-propanol saturated with HCl was added (7 mL). The resulting white precipitate was filtered, washed with diethyl ether, and dried under vacuum to afford **33**. Mp = 130°C. Yield = 88%. IR (υ, cm^{-1}): 2474 (NH^+), 1733 (C=O), 1529 (NO_2). ^1H NMR (DMSO, 300 MHz) δ ppm: 1.23-1.27 (m, 6H, $2NCH_2CH_3$), 3.20-3.23 (m, 4H, $2NCH_2CH_3$), 3.52-3.54 (m, 2H, NCH_2CH_2O), 3.84 (s, 3H, OCH_3), 3.95 (s, 3H, OCH_3), 4.49-4.53 (m, 2H, NCH_2CH_2O), 7.39 (s, 1H, ArH), 7.77 (s, 1H, ArH), 9.98 (s, 1H, NH^+). LC/MS (ESI^+) *m/z* 327 $(M+H)^+$.

Methyl 2-amino-4-(2-(diethylamino)ethoxy)-5-methoxybenzoate hydrochloride (34)

Compound **33** (6 mmol) was dissolved in methanol (50 mL), and Raney nickel (0.4 g) was added. The mixture was stirred under a hydrogen atmosphere at room temperature for 16 h. The

product was passed through a plug of Celite before being concentrated and purified by column chromatography on silica gel eluting with CH_2Cl_2/MeOH (9/1). Petroleum ether provided the title compound as a brown solid. Mp = 177°C. Yield = 66%. IR (υ, cm^{-1}): 3265 (NH_2), 2462 (NH^+), 2679 (C=O). ^1H NMR (DMSO, 300 MMHz) δ ppm: 1.25-1.29 (m, 6H, $2NCH_2CH_3$), 3.21-3.23 (m, 4H, $2NCH_2CH_3$), 3.50-3.54 (m, 2H, NCH_2CH_2O), 3.67 (s, 3H, OCH_3), 3.76 (s, 3H, OCH_3), 4.34-4.37 (t, 2H, NCH_2CH_2O, *J* = 4.60 Hz), 6.41 (s, 1H, ArH), 6.50 (s, 2H, NH_2), 7.17 (s, 1H, ArH), 10.76 (s, 1H, NH^+). LC/MS (ESI^+) *m/z* 297 $(M+H)^+$.

7-(2-(diethylamino)ethoxy)-6-methoxyquinazolin-4(3H)-one (35)

A mixture of **34** (3 mmol) and ammonium formate (9 mmol, 3 equiv.) in formamide (1 mL) was heated at 140°C for 16 h. The reaction was hydrolyzed with potassium carbonate solution (1 N, 40 mL) and extracted with ethyl acetate (5 × 30 mL). The combined organic layers were dried over magnesium sulfate and concentrated under vacuum. The residue was purified by column chromatography on silica gel eluting with CH_2Cl_2/MeOH (9/1) to give a brown solid. Mp = 138°C. Yield = 68%. IR (υ, cm^{-1}): 1660 (C=O), 1608 (NH). ^1H NMR (DMSO, 300 MHz) δ ppm: 0.96-1.01 (m, 6H, $2NCH_2CH_3$), 2.58-2.60 (m, 4H, $2NCH_2CH_3$), 2.81-2.86 (t, 2H, NCH_2CH_2O, *J* = 6.0 Hz), 3.87 (s, 3H, OCH_3), 4.13-4.18 (t, 2H, NCH_2CH_2O, *J* = 6.0 Hz), 7.15 (s, 1H, ArH), 7.44 (s, 1H, ArH), 7.98 (s, 1H, ArH), 12.07 (s, 1H, OH). LC/MS (ESI^+) *m/z* 292 $(M+H)^+$.

2-((4-chloro-6-methoxyquinazolin-7-yl)oxy)-N,N-diethylethanamine (36)

A mixture of **35** (3 mmol) and phosphorous oxychloride (20 mL) was refluxed for 2 h. After evaporation under vacuum, ice water (50 mL) was added and the mixture was neutralized by ammonium hydroxide. The aqueous layer was extracted with CH_2Cl_2 (3 × 50 mL) and the extract was washed with saturated aqueous sodium hydrogen carbonate solution and dried over calcium chloride. The solvent was removed by evaporation and the residue was purified by

column chromatography on silica gel eluting with CH_2Cl_2/MeOH (9/1) to provide a white solid. Mp = 190°C. Yield = 95%. IR (υ, cm^{-1}): 1160 (C-Cl). ^1H NMR (DMSO, 300 MHz) δ ppm: 1.04-1.09 (m, 6H, $2NCH_2CH_3$), 2.67-2.82 (m, 4H, $2NCH_2CH_3$), 2.96-3.12 (m, 2H, NCH_2CH_2O), 3.92 (s, 3H, OCH_3), 4.11 (s, 3H, OCH_3), 4.25-4.35 (m, 2H, NCH_2CH_2O), 7.34 (s, 1H, ArH), 7.36 (s, 1H, ArH), 8.64 (s, 1H, ArH). LC/MS (ESI^+) *m/z* 310 $(M+H)^+$.

N-(2,4-dichloro-5-methoxyphenyl)-7-(2-(diethylamino)ethoxy)-6-methoxyquinazolin-4-amine (37)

Compound **37** was synthesized using method b and after crystallization from acetonitrile, was isolated as a white solid. Mp = 169°C. Yield = 27 %. IR (υ, cm^{-1}): 1600 (NH), 1079 (C-Cl). ^1H NMR (DMSO, 300 MHz) δ ppm: 0.99-1.03 (m, 6H, $2NCH_2CH_3$), 2.56-2.62 (m, 4H, $2NCH_2CH_3$), 2.85-2.89 (t, 2H, NCH_2CH_2O, *J* = 6.0 Hz), 3.87 (s, 3H, OCH_3), 3.94 (s, 3H, OCH_3), 4.48-4.22 (t, 2H, NCH_2CH_2O, *J* = 6.0 Hz), 7.21 (s, 1H, ArH), 7.36 (s, 1H, ArH), 7.71 (s, 1H, ArH), 7.83 (s, 1H, ArH), 8.34 (s, 1H, ArH), 9.60 (s, 1H, NH). ^{13}C NMR (DMSO, 75 MHz) δ ppm: 157.8 (C), 154.1 (C), 154.0 (C), 153.5 (CH), 149.5 (C), 147.4 (C), 136.8 (C), 130.2 (CH), 123.0 (C), 119.5 (C), 114.0 (CH), 109.0 (C), 108.2 (CH), 102.4 (CH), 67.7 (CH_2), 57.1 (CH_3), 56.6 (CH_3), 51.4 (CH_2), 47.5 ($2CH_2$), 12.3 ($2CH_3$). LC/MS (ESI^+) *m/z* 465 $(M+H)^+$.

Methyl 3-(2-(diethylamino)ethoxy)-4-methoxybenzoate hydrochloride (38)

Compound **38** was obtained by the same procedure as used for **32**. Starting from methyl 3-hydroxy-4-methoxybenzoate (0.08 mol), a white solid was synthesized. Mp = 104 °C. Yield = 77%. IR (υ, cm^{-1}): 2454 (NH^+), 1714 (C=O). ^1H NMR (DMSO, 300 MHz) δ ppm: 1.23-1.29 (m, 6H, $2NCH_2CH_3$), 3.20-3.25 (m, 4H, $2NCH_2CH_3$), 3.48-3.50 (m, 2H, NCH_2CH_2O), 3.82 (s, 3H, OCH_3), 3.85 (s, 3H, OCH_3), 4.50 (t, 2H, NCH_2CH_2O, *J* = 4.7 Hz), 7.11-7.14 (d, 1H, ArH, *J* = 8.6 Hz), 7.50-7.51 (d, 1H, ArH, *J* = 1.8 Hz), 7.63-7.67 (dd, 1H, ArH, *J* = 8.5 Hz and *J* = 1.8 Hz), 10.69 (s, 1H, NH^+). LC/MS (ESI^+) *m/z* 282 $(M+H)^+$.

Methyl 5-(2-(diethylamino)ethoxy)-4-methoxy-2-nitrobenzoate hydrochloride (39)

A solution of tin (IV) chloride (28 mmol) and nitric fuming acid (28 mmol) in CH_2Cl_2 (20 mL) was added dropwise to a solution of **38** (9.40 mmol) in CH_2Cl_2 (150 mL) cooled at -70°C. After stirring for 8h at -70°C and warming to room temperature, water was added (100 mL). The aqueous layer was basified with 6 N NaOH and extracted with CH_2Cl_2 (3 × 70 mL). The combined organic layers were washed with saturated potassium carbonate solution and saturated sodium chloride solution and dried over calcium chloride. After concentration under vacuum, the oily residue was dissolved in 2-propanol (3 mL), and 2-propanol saturated with HCl was added (7 mL). The resulting white precipitate was filtered, washed with diethyl ether, and dried under vacuum to afford **39**. Mp = 135°C. Yield = 91%. IR (υ, cm^{-1}): 2484 (NH^+), 1710 (C=O), 1520 (NO_2). ^{1}H NMR (DMSO, 300 MHz) δ ppm: 1.24-1.29 (m, 6H, 2NCH$_2$*CH*$_3$), 3.21-3.23 (m, 4H, 2N*CH*$_2$CH$_3$), 3.54-3.56 (m, 2H, N*CH*$_2$CH$_2$O), 3.84 (s, 3H, OCH$_3$), 3.93 (s, 3H, OCH$_3$), 4.53-4.57 (t, 2H, NCH$_2$*CH*$_2$O, *J* = 4.8 Hz), 7.43 (s, 1H, ArH), 7.70 (s, 1H, ArH), 10.56 (s, 1H, NH^+). LC/MS (ESI^+) *m/z* 327 $(M+H)^+$.

Methyl 2-amino-5-(2-(diethylamino)ethoxy)-4-methoxybenzoate hydrochloride (40)

Compound **40** was obtained by using the same procedure as used for **34**. Starting from **39** (6 mmol), a brown solid was obtained after purification by column chromatography on silica gel eluting with CH_2Cl_2/CH_3OH (9/1). Mp = 144°C. Yield = 77%. IR (υ, cm^{-1}): 3447 (NH_2), 2453 (NH^+), 1680 (C=O). ^{1}H NMR (DMSO, 300 MHz) δ ppm: 1.23-1.28 (m, 6H, 2NCH$_2$*CH*$_3$), 3.20-3.27 (m, 4H, 2N*CH*$_2$CH$_3$), 3.41-3.45 (m, 2H, N*CH*$_2$CH$_2$O), 3.76 (s, 3H, OCH$_3$), 3.78 (s, 3H, OCH$_3$), 4.17-4.20 (t, 2H, NCH$_2$*CH*$_2$O, *J* = 4.8 Hz), 6.42 (s, 1H, ArH), 6.57 (s, 2H, NH_2), 7.27 (s, 1H, ArH), 10.18 (s, 1H, NH^+). LC/MS (ESI^+) *m/z* 297 $(M+H)^+$.

6-(2-(diethylamino)ethoxy)-7-methoxyquinazolin-4(3H)-one (41)

A mixture of **40** (3 mmol) and ammonium formate (9 mmol, 3 equiv.) in formamide (1 mL) was heated at 140°C for 16 h. The reaction was treated with water (50 mL) and extracted with CH_2Cl_2 (2 × 30 mL). The aqueous layer was neutralized by a saturated potassium carbonate solution. The precipitate was collected by filtration and washed with water and diethyl ether to provide a white solid after crystallization from ethanol. Mp = 235°C. Yield = 71%. IR (υ, cm^{-1}): 1670 (C=O), 1612 (NH). ^{1}H NMR (DMSO, 300 MHz) δ ppm: 0.96-1.01 (m, 6H, $2NCH_2CH_3$), 2.51-2.65 (m, 4H, $2NCH_2CH_3$), 2.83-2.89 (m, 2H, NCH_2CH_2O), 3.91 (s, 3H, OCH_3), 4.06-4.16 (m, 2H, NCH_2CH_2O), 7.14 (s, 1H, ArH), 7.46 (s, 1H, ArH), 7.99 (s, 1H, ArH), 12.06 (s, 1H, OH). LC/MS (ESI^+) *m/z* 292 $(M+H)^+$.

2-((4-chloro-7-methoxyquinazolin-6-yl)oxy)-N,N-diethylethanamine (42)

Compound **42** was obtained by using the same procedure as used for **36**. Starting from **41** (3 mmol), a white solid was prepared after purification by column chromatography on silica gel eluting with CH_2Cl_2/CH_3OH (95/5). Mp = 202°C. Yield = 92%. IR (υ, cm^{-1}): 1614 (NH), 1158 (C-Cl). ^{1}H NMR (DMSO, 300 MHz) δ ppm: 0.99-1.04 (m, 6H, $2NCH_2CH_3$), 2.60-2.63 (m, 4H, $2NCH_2CH_3$), 2.88-2.93 (m, 2H, NCH_2CH_2O), 4.02 (s, 3H, OCH_3), 4.24-4.28 (t, 2H, NCH_2CH_2O, *J* = 5.8 Hz), 7.45 (s, 1H, ArH), 7.46 (s, 1H, ArH), 8.89 (s, 1H, ArH). LC/MS (ESI^+) *m/z* 310 $(M+H)^+$.

N-(2,4-dichloro-5-methoxyphenyl)-6-(2-(diethylamino)ethoxy)-7-methoxyquinazolin-4-amine (43)

Compound **43** was synthesized using method b and was isolated as a white solid. Mp = 175°C. Yield = 49 %. IR (υ, cm^{-1}): 1603 (NH), 1077 (C-Cl). ^{1}H NMR (DMSO, 300 MHz) δ ppm: 1.00-1.05 (m, 6H, $2NCH_2CH_3$), 2.61-2.66 (m, 4H, $2NCH_2CH_3$), 2.87-2.94 (m, 2H, NCH_2CH_2O), 3.87 (s, 3H, OCH_3), 3.94 (s, 3H, OCH_3), 4.15-4.20 (m 2H, NCH_2CH_2O), 7.20 (s, 1H, ArH), 7.36 (s, 1H, ArH), 7.71 (s, 1H, ArH), 7.84 (s, 1H, ArH), 8.34 (s, 1H, ArH), 9.58

(s, 1H, NH). ^{13}C NMR (DMSO, 75 MHz) δ ppm: 157.8 (C), 154.9 (C), 154.1 (C), 153.5 (CH), 148.6 (C), 147.4 (C), 136.8 (C), 130.2 (CH), 123.1 (C), 119.6 (C), 114.1 (CH), 109.0 (C), 107.6 (CH), 103.0 (CH), 67.9 (CH_2), 57.1 (CH_3), 56.3 (CH_3), 51.7 (CH_2), 47.6 ($2CH_2$), 12.3 ($2CH_3$). LC/MS (ESI^+) *m/z* 465 $(M+H)^+$.

Methyl 2-amino-4-(2-(diethylamino)ethoxy)benzoate (44)

Potassium carbonate (0.24 mmol) was added to a solution of methyl 2-amino-4-hydroxybenzoate (0.06 mmol, 4 equiv.) in acetone (20 mL) and was stirred for 5 min. 2-diethylaminoethyl chloride hydrochloride (0.06 mmol) was added and the mixture was refluxed for 16 h. The inorganic solid was filtered off and the filtrate was concentrated under vacuum to afford compound **44** as a yellow oil. Yield = 94%. IR (υ, cm^{-1}): 3147 (NH_2), 1682 (C=O), 1224 (C-O-C). ^{1}H NMR (DMSO, 300 MHz) δ ppm: 0.95-1.00 (m, 6H, $2NCH_2CH_3$), 2.55-2.58 (m, 4H, $2NCH_2CH_3$), 2.74-2.78 (t, 2H, NCH_2CH_2O, *J* = 5.8 Hz), 3.74 (s, 3H, OCH_3), 4.43-4.47 (t, 2H, NCH_2CH_2O, *J* = 6.1 Hz), 6.11-6.15 (dd, 1H, ArH, *J* = 8.7 Hz and *J* = 9.0 Hz), 6.27-6.28 (d, 1H, ArH, *J* = 2.4 Hz), 6.68 (s, 2H, NH_2), 7.60-7.63 (d, 1H, ArH, *J* = 9.0 Hz). LC/MS (ESI^+) *m/z* 267 $(M+H)^+$.

7-(2-(diethylamino)ethoxy)quinazolin-4(3H)-one (45)

Compound **45** was obtained by the same procedure as used for **35**. Starting from **44** (0.06 mmol), a white solid was synthesized. Mp > 250 °C. Yield = 68%. IR (υ, cm^{-1}): 2965 (OH), 1607 (C=N). ^{1}H-NMR (DMSO, 300 MHz) δ ppm: 0.96-1.00 (m, 6H, $2NCH_2CH_3$), 2.53-2.59 (m, 4H, $2NCH_2CH_3$), 2.79-2.83 (t, 2H, NCH_2CH_2O, *J* = 6.0 Hz), 4.11-4.15 (t, 2H, NCH_2CH_2O, *J* = 6.0 Hz), 7.04-7.05 (d, 1H, ArH, *J* = 2.4 Hz), 7.08 (S, 1H, ArH), 7.98-8.01 (m, 1H, ArH), 8.05 (s, 1H, ArH), 12.05 (s, 1H, OH). LC/MS (ESI^+) *m/z* 262 $(M+H)^+$.

2-((4-chloroquinazolin-7-yl)oxy)-N,N-diethylethanamine (46)

Compound **46** was obtained by the same procedure as used for **36**. Starting from **45** (0.04 mmol), a white solid was synthesized. Mp = 62 °C. Yield = 31%. IR (υ, cm^{-1}): 1142 (C-Cl). ^{1}H-NMR (DMSO, 300 MHz) δ ppm: 0.97-1.02 (m, 6H, $2NCH_2CH_3$), 2.56-2.63 (m, 4H, $2NCH_2CH_3$), 2.86-2.90 (m, 2H, NCH_2CH_2O), 4.27-4.31 (t, 2H, NCH_2CH_2O, *J* = 6.0 Hz), 7.46-7.50 (m, 2H, ArH), 8.16-8.19 (m, 1H, ArH), 8.99 (s, 1H, ArH). LC/MS (ESI^+) *m/z* 280 $(M+H)^+$.

N-(2,4-dichloro-5-methoxyphenyl)-7-(2-(diethylamino)ethoxy)quinazolin-4-amine (47)

Compound **47** was obtained using method b and was isolated as a beige solid. Mp = 210 °C. Yield = 16%. IR (υ, cm^{-1}): 3428 (NH), 1217 (C-O-C), 1158 (C-Cl). ^{1}H-NMR (DMSO, 300 MHz) δ ppm: 1.01-1.11 (m, 6H, $2NCH_2CH_3$), 2.64-2.81 (m, 4H, $2NCH_2CH_3$), 2.93-3.04 (m, 2H, NCH_2CH_2O), 3.88 (s, 3H, OCH_3), 4.23-4.31 (m, 2H, NCH_2CH_2O), 7.21-7.27 (m, 2H, ArH), 7.40 (s, 1H, ArH), 7.70 (s, 1H, ArH), 8.37-8.42 (m, 2H, ArH), 9.81 (s, 1H, NH). ^{13}C NMR (DMSO, 75 MHz) δ ppm: 162.4 (C), 158.8 (C), 155.7 (CH), 154.1 (C), 152.5 (C), 136.6 (C), 130.2 (CH), 125.2 (CH), 123.1 (C), 119.7 (C), 118.4 (CH), 114.1 (CH), 109.5 (C), 108.1 (CH), 57.1 (CH_3), 51.4 ($2CH_2$), 47.5 ($2CH_2$), 11.8 ($2CH_3$). LC/MS (ESI^+) *m/z* 435 $(M+H)^+$.

10. AUTHOR CONTRIBUTIONS

The manuscript was written through contributions of all authors. All authors have given approval to the final version of the manuscript.

11. FUNDING

We gratefully acknowledge the “Ecole Doctorale Biologie-Santé de Lille” for doctoral research allowance to Morgane Rivoal and the financial support of StartAIRR from "Région Hauts de France".

12. BIBLIOGRAPHY

[1] F.G. Bauernfeind, G. Horvath, A. Stutz, E.S. Alnemri, K. MacDonald, D. Speert, T. Fernandes-Alnemri, J. Wu, B.G. Monks, K.A. Fitzgerald, V. Hornung, E. Latz, Cutting Edge: NF-κB Activating Pattern Recognition and Cytokine Receptors License NLRP3 Inflammasome Activation by Regulating NLRP3 Expression, J. Immunol. 183 (2009) 787–791. https://doi.org/10.4049/jimmunol.0901363.

[2] L.S. Murillo, S.A. Morré, A.S. Peña, Toll-like receptors and NOD/CARD proteins: pattern recognition receptors are key elements in the regulation of immune response, Drugs Today Barc. Spain 1998 39 (2003) 415–438.
[3] P. Tourlomousis, J.A. Wright, A.S. Bittante, L.J. Hopkins, S.J. Webster, O.J. Bryant, P. Mastroeni, D.J. Maskell, C.E. Bryant, Modifying bacterial flagellin to evade Nod-like Receptor CARD 4 recognition enhances protective immunity against Salmonella, Nat. Microbiol. 5 (2020) 1588–1597. https://doi.org/10.1038/s41564-020-00801-y.
[4] T. Watanabe, N. Asano, S. Fichtner-Feigl, P.L. Gorelick, Y. Tsuji, Y. Matsumoto, T. Chiba, I.J. Fuss, A. Kitani, W. Strober, NOD1 contributes to mouse host defense against Helicobacter pylori via induction of type I IFN and activation of the ISGF3 signaling pathway, J. Clin. Invest. 120 (2010) 1645–1662. https://doi.org/10.1172/JCI39481.
[5] W. Strober, P.J. Murray, A. Kitani, T. Watanabe, Signalling pathways and molecular interactions of NOD1 and NOD2, Nat. Rev. Immunol. 6 (2006) 9–20. https://doi.org/10.1038/nri1747.
[6] A.K. Pandey, Y. Yang, Z. Jiang, S.M. Fortune, F. Coulombe, M.A. Behr, K.A. Fitzgerald, C.M. Sassetti, M.A. Kelliher, NOD2, RIP2 and IRF5 play a critical role in the type I interferon response to Mycobacterium tuberculosis, PLoS Pathog. 5 (2009) e1000500. https://doi.org/10.1371/journal.ppat.1000500.
[7] L. Moreno, T. Gatheral, Therapeutic targeting of NOD1 receptors, Br. J. Pharmacol. 170 (2013) 475–485. https://doi.org/10.1111/bph.12300.
[8] P. Hruz, L. Eckmann, Caspase recruitment domain-containing sensors and adaptors in intestinal innate immunity, Curr. Opin. Gastroenterol. 24 (2008) 108–114. https://doi.org/10.1097/MOG.0b013e3282f50fdf.
[9] M. Fernández-Velasco, P. Prieto, V. Terrón, G. Benito, J.M. Flores, C. Delgado, C. Zaragoza, B. Lavin, M. Gómez-Parrizas, E. López-Collazo, P. Martín-Sanz, L. Boscá, NOD1 activation induces cardiac dysfunction and modulates cardiac fibrosis and cardiomyocyte apoptosis, PloS One 7 (2012) e45260. https://doi.org/10.1371/journal.pone.0045260.
[10] L. Chen, R. Chen, H. Wang, F. Liang, Mechanisms Linking Inflammation to Insulin Resistance, Int. J. Endocrinol. 2015 (2015) 508409. https://doi.org/10.1155/2015/508409.
[11] N. Dali-Youcef, M. Mecili, R. Ricci, E. Andrès, Metabolic inflammation: connecting obesity and insulin resistance, Ann. Med. 45 (2013) 242–253. https://doi.org/10.3109/07853890.2012.705015.
[12] S.L. Rivers, A. Klip, A. Giacca, NOD1: An Interface Between Innate Immunity and Insulin Resistance, Endocrinology 160 (2019) 1021–1030. https://doi.org/10.1210/en.2018-01061.
[13] L. Zhao, P. Hu, Y. Zhou, J. Purohit, D. Hwang, NOD1 activation induces proinflammatory gene expression and insulin resistance in 3T3-L1 adipocytes, Am. J. Physiol. Endocrinol. Metab. 301 (2011) E587-598. https://doi.org/10.1152/ajpendo.00709.2010.
[14] J. Amar, C. Chabo, A. Waget, P. Klopp, C. Vachoux, L.G. Bermúdez-Humarán, N. Smirnova, M. Bergé, T. Sulpice, S. Lahtinen, A. Ouwehand, P. Langella, N. Rautonen, P.J. Sansonetti, R. Burcelin, Intestinal mucosal adherence and translocation of commensal bacteria at the early onset of type 2 diabetes: molecular mechanisms and probiotic treatment, EMBO Mol. Med. 3 (2011) 559–572. https://doi.org/10.1002/emmm.201100159.
[15] J.D. Schertzer, A.K. Tamrakar, J.G. Magalhães, S. Pereira, P.J. Bilan, M.D. Fullerton, Z. Liu, G.R. Steinberg, A. Giacca, D.J. Philpott, A. Klip, NOD1 activators link innate immunity to insulin resistance, Diabetes 60 (2011) 2206–2215. https://doi.org/10.2337/db11-0004.
[16] P.M. Khan, R.G. Correa, D.B. Divlianska, S. Peddibhotla, E.H. Sessions, G. Magnuson, B. Brown, E. Suyama, H. Yuan, A. Mangravita-Novo, M. Vicchiarelli, Y. Su, S. Vasile, L.H. Smith, P.W. Diaz, J.C. Reed, G.P. Roth, Identification of Inhibitors of NOD1-Induced Nuclear Factor-κB Activation, ACS Med. Chem. Lett. 2 (2011) 780–785. https://doi.org/10.1021/ml200158b.
[17] D.J. Rickard, C.A. Sehon, V. Kasparcova, L.A. Kallal, P.A. Haile, X. Zeng, M.N. Montoute, D.D. Poore, H. Li, Z. Wu, P.M. Eidam, J.G. Emery, R.W. Marquis, P.J. Gough, J. Bertin, Identification of Selective Small Molecule Inhibitors of the Nucleotide-Binding Oligomerization Domain 1 (NOD1) Signaling Pathway, PLoS ONE 9 (2014) e96737. https://doi.org/10.1371/journal.pone.0096737.

[18] R.G. Correa, P.M. Khan, N. Askari, D. Zhai, M. Gerlic, B. Brown, G. Magnuson, R. Spreafico, S. Albani, E. Sergienko, P.W. Diaz, G.P. Roth, J.C. Reed, Discovery and Characterization of 2-Aminobenzimidazole Derivatives as Selective NOD1 Inhibitors, Chem. Biol. 18 (2011) 825–832. https://doi.org/10.1016/j.chembiol.2011.06.009.
[19] C. Russo, P. Russomanno, V.M. D'Amore, A.I. Alfano, F. Santoro, S. Guzelj, M. Gobec, J. Amato, B. Pagano, L. Marinelli, A. Carotenuto, G.C. Tron, F.S. Di Leva, Ž. Jakopin, D. Brancaccio, M. Giustiniano, Discovery of 2,3-Diaminoindole Derivatives as a Novel Class of NOD Antagonists, J. Med. Chem. 67 (2024) 3004–3017. https://doi.org/10.1021/acs.jmedchem.3c02094.
[20] Ž. Jakopin, Nucleotide-Binding Oligomerization Domain (NOD) Inhibitors: A Rational Approach toward Inhibition of NOD Signaling Pathway, J. Med. Chem. 57 (2014) 6897–6918. https://doi.org/10.1021/jm401841p.
[21] J.T. Tigno-Aranjuez, P. Benderitter, F. Rombouts, F. Deroose, X. Bai, B. Mattioli, F. Cominelli, T.T. Pizarro, J. Hoflack, D.W. Abbott, In Vivo Inhibition of RIPK2 Kinase Alleviates Inflammatory Disease, J. Biol. Chem. 289 (2014) 29651–29664. https://doi.org/10.1074/jbc.M114.591388.
[22] P. Canning, Q. Ruan, T. Schwerd, M. Hrdinka, J.L. Maki, D. Saleh, C. Suebsuwong, S. Ray, P.E. Brennan, G.D. Cuny, H.H. Uhlig, M. Gyrd-Hansen, A. Degterev, A.N. Bullock, Inflammatory Signaling by NOD-RIPK2 Is Inhibited by Clinically Relevant Type II Kinase Inhibitors, Chem. Biol. 22 (2015) 1174–1184. https://doi.org/10.1016/j.chembiol.2015.07.017.
[23] U. Nachbur, C.A. Stafford, A. Bankovacki, Y. Zhan, L.M. Lindqvist, B.K. Fiil, Y. Khakham, H.-J. Ko, J.J. Sandow, H. Falk, J.K. Holien, D. Chau, J. Hildebrand, J.E. Vince, P.P. Sharp, A.I. Webb, K.A. Jackman, S. Mühlen, C.L. Kennedy, K.N. Lowes, J.M. Murphy, M. Gyrd-Hansen, M.W. Parker, E.L. Hartland, A.M. Lew, D.C.S. Huang, G. Lessene, J. Silke, A RIPK2 inhibitor delays NOD signalling events yet prevents inflammatory cytokine production, Nat. Commun. 6 (2015) 6442. https://doi.org/10.1038/ncomms7442.
[24] X. Yuan, Y. Chen, M. Tang, Y. Wei, M. Shi, Y. Yang, Y. Zhou, T. Yang, J. Liu, K. Liu, D. Deng, C. Zhang, L. Chen, Discovery of Potent and Selective Receptor-Interacting Serine/Threonine Protein Kinase 2 (RIPK2) Inhibitors for the Treatment of Inflammatory Bowel Diseases (IBDs), J. Med. Chem. 65 (2022) 9312–9327. https://doi.org/10.1021/acs.jmedchem.2c00604.
[25] P.A. Haile, B.J. Votta, R.W. Marquis, M.J. Bury, J.F. Mehlmann, R. Singhaus, A.K. Charnley, A.S. Lakdawala, M.A. Convery, D.B. Lipshutz, B.M. Desai, B. Swift, C.A. Capriotti, S.B. Berger, M.K. Mahajan, M.A. Reilly, E.J. Rivera, H.H. Sun, R. Nagilla, A.M. Beal, J.N. Finger, M.N. Cook, B.W. King, M.T. Ouellette, R.D. Totoritis, M. Pierdomenico, A. Negroni, L. Stronati, S. Cucchiara, B. Ziółkowski, A. Vossenkämper, T.T. MacDonald, P.J. Gough, J. Bertin, L.N. Casillas, The Identification and Pharmacological Characterization of 6-(tert-Butylsulfonyl)-N-(5-fluoro-1H-indazol-3-yl)quinolin-4-amine (GSK583), a Highly Potent and Selective Inhibitor of RIP2 Kinase, J. Med. Chem. 59 (2016) 4867–4880. https://doi.org/10.1021/acs.jmedchem.6b00211.
[26] X. He, S. Da Ros, J. Nelson, X. Zhu, T. Jiang, B. Okram, S. Jiang, P.-Y. Michellys, M. Iskandar, S. Espinola, Y. Jia, B. Bursulaya, A. Kreusch, M.-Y. Gao, G. Spraggon, J. Baaten, L. Clemmer, S. Meeusen, D. Huang, R. Hill, V. Nguyen-Tran, J. Fathman, B. Liu, T. Tuntland, P. Gordon, T. Hollenbeck, K. Ng, J. Shi, L. Bordone, H. Liu, Identification of Potent and Selective RIPK2 Inhibitors for the Treatment of Inflammatory Diseases, ACS Med. Chem. Lett. 8 (2017) 1048–1053. https://doi.org/10.1021/acsmedchemlett.7b00258.
[27] A.K. Charnley, M.A. Convery, A. Lakdawala Shah, E. Jones, P. Hardwicke, A. Bridges, M. Ouellette, R. Totoritis, B. Schwartz, B.W. King, D.D. Wisnoski, J. Kang, P.M. Eidam, B.J. Votta, P.J. Gough, R.W. Marquis, J. Bertin, L. Casillas, Crystal structures of human RIP2 kinase catalytic domain complexed with ATP-competitive inhibitors: Foundations for understanding inhibitor selectivity, Bioorg. Med. Chem. 23 (2015) 7000–7006. https://doi.org/10.1016/j.bmc.2015.09.038.
[28] M. Hrdinka, L. Schlicher, B. Dai, D.M. Pinkas, J.C. Bufton, S. Picaud, J.A. Ward, C. Rogers, C. Suebsuwong, S. Nikhar, G.D. Cuny, K.V. Huber, P. Filippakopoulos, A.N. Bullock, A. Degterev, M. Gyrd-Hansen, Small molecule inhibitors reveal an indispensable scaffolding role of RIPK2 in NOD2 signaling, EMBO J. 37 (2018) e99372. https://doi.org/10.15252/embj.201899372.

[29] S. Nikhar, I. Siokas, L. Schlicher, S. Lee, M. Gyrd-Hansen, A. Degterev, G.D. Cuny, Design of pyrido[2,3-d]pyrimidin-7-one inhibitors of receptor interacting protein kinase-2 (RIPK2) and nucleotide-binding oligomerization domain (NOD) cell signaling, Eur. J. Med. Chem. 215 (2021) 113252. https://doi.org/10.1016/j.ejmech.2021.113252.
[30] J. Ermann, M. Matmusaev, E.K. Haley, C. Braun, F. Jost, S. Mayer-Wrangowski, P. Hsiao, N. Ting, L. Li, D. Terenzio, J. Chime, S. Lukas, L. Patnaude, M. Panzenbeck, D. Csordas, J. Zheng, D. Mierz, T. Simpson, F.J. King, A.P. Klimowicz, M.L. Mbow, J.S. Fine, C.A. Miller, S.E. Fogal, F.R. Byrne, The potent and selective RIPK2 inhibitor BI 706039 improves intestinal inflammation in the TRUC mouse model of inflammatory bowel disease, Am. J. Physiol.-Gastrointest. Liver Physiol. 321 (2021) G500–G512. https://doi.org/10.1152/ajpgi.00163.2021.
[31] Oncodesign, ONCODESIGN strengthens the intellectual property of ODS 101 in treating inflammatory bowel disease, Oncodesign (n.d.). https://www.oncodesign.com/cpt_ressource/oncodesign-strengthens-the-intellectual-property-of-ods-101-in-treating-inflammatory-bowel-disease/ (accessed June 24, 2022).
[32] D.E. Thurston, D.S. Bose, A.S. Thompson, P.W. Howard, A. Leoni, S.J. Croker, T.C. Jenkins, S. Neidle, J.A. Hartley, L.H. Hurley, Synthesis of Sequence-Selective C8-Linked Pyrrolo[2,1-c][1,4]benzodiazepine DNA Interstrand Cross-Linking Agents, J. Org. Chem. 61 (1996) 8141–8147. https://doi.org/10.1021/jo951631s.
[33] P.A. Haile, L.N. Casillas, B.J. Votta, G.Z. Wang, A.K. Charnley, X. Dong, M.J. Bury, J.J. Romano, J.F. Mehlmann, B.W. King, K.F. Erhard, C.R. Hanning, D.B. Lipshutz, B.M. Desai, C.A. Capriotti, M.C. Schaeffer, S.B. Berger, M.K. Mahajan, M.A. Reilly, R. Nagilla, E.J. Rivera, H.H. Sun, J.K. Kenna, A.M. Beal, M.T. Ouellette, M. Kelly, G. Stemp, M.A. Convery, A. Vossenkämper, T.T. MacDonald, P.J. Gough, J. Bertin, R.W. Marquis, Discovery of a First-in-Class Receptor Interacting Protein 2 (RIP2) Kinase Specific Clinical Candidate, 2-((4-(Benzo[*d*]thiazol-5-ylamino)-6-(*tert* -butylsulfonyl)quinazolin-7-yl)oxy)ethyl Dihydrogen Phosphate, for the Treatment of Inflammatory Diseases, J. Med. Chem. 62 (2019) 6482–6494. https://doi.org/10.1021/acs.jmedchem.9b00575.
[34] R. Caruso, N. Warner, N. Inohara, G. Núñez, NOD1 and NOD2: Signaling, Host Defense, and Inflammatory Disease, Immunity 41 (2014) 898–908. https://doi.org/10.1016/j.immuni.2014.12.010.
[35] F. Ciardiello, T. Troiani, R. Bianco, M. Orditura, F. Morgillo, E. Martinelli, M.P. Morelli, T. Cascone, G. Tortora, Interaction between the epidermal growth factor receptor (EGFR) and the vascular endothelial growth factor (VEGF) pathways: a rational approach for multi-target anticancer therapy, Ann. Oncol. 17 (2006) vii109–vii114. https://doi.org/10.1093/annonc/mdl962.
[36] E. Pellegrini, L. Signor, S. Singh, E.B. Erba, S. Cusack, Structures of the inactive and active states of RIP2 kinase inform on the mechanism of activation, PLOS ONE 12 (2017) e0177161. https://doi.org/10.1371/journal.pone.0177161.
[37] E. Pellegrini, A. Desfosses, A. Wallmann, W.M. Schulze, K. Rehbein, P. Mas, L. Signor, S. Gaudon, G. Zenkeviciute, M. Hons, H. Malet, I. Gutsche, C. Sachse, G. Schoehn, H. Oschkinat, S. Cusack, RIP2 filament formation is required for NOD2 dependent NF-κB signalling, Nat. Commun. 9 (2018) 4043. https://doi.org/10.1038/s41467-018-06451-3.
[38] R.B. Damgaard, U. Nachbur, M. Yabal, W.W.-L. Wong, B.K. Fiil, M. Kastirr, E. Rieser, J.A. Rickard, A. Bankovacki, C. Peschel, J. Ruland, S. Bekker-Jensen, N. Mailand, T. Kaufmann, A. Strasser, H. Walczak, J. Silke, P.J. Jost, M. Gyrd-Hansen, The Ubiquitin Ligase XIAP Recruits LUBAC for NOD2 Signaling in Inflammation and Innate Immunity, Mol. Cell 46 (2012) 746–758. https://doi.org/10.1016/j.molcel.2012.04.014.
[39] T. Goncharov, S. Hedayati, M.M. Mulvihill, A. Izrael-Tomasevic, K. Zobel, S. Jeet, A.V. Fedorova, C. Eidenschenk, J. deVoss, K. Yu, A.S. Shaw, D.S. Kirkpatrick, W.J. Fairbrother, K. Deshayes, D. Vucic, Disruption of XIAP-RIP2 Association Blocks NOD2-Mediated Inflammatory Signaling, Mol. Cell 69 (2018) 551-565.e7. https://doi.org/10.1016/j.molcel.2018.01.016.

[40] S. Mayle, J.P. Boyle, E. Sekine, B. Zurek, T.A. Kufer, T.P. Monie, Engagement of nucleotide-binding oligomerization domain-containing protein 1 (NOD1) by receptor-interacting protein 2 (RIP2) is insufficient for signal transduction, J. Biol. Chem. 289 (2014) 22900–22914. https://doi.org/10.1074/jbc.M114.557900.
[41] V. Fridh, K. Rittinger, The tandem CARDs of NOD2: intramolecular interactions and recognition of RIP2, PloS One 7 (2012) e34375. https://doi.org/10.1371/journal.pone.0034375.
[42] Y. Li, X. Chen, W. Li, Y. Ye, X. Du, S. Sun, L. Liu, H. Zhang, Combination of Anti-EGFR and Anti-VEGF Drugs for the Treatment of Previously Treated Metastatic Colorectal Cancer: A Case Report and Literature Review, Front. Oncol. 11 (2021) 684309. https://doi.org/10.3389/fonc.2021.684309.
[43] C. Ding, L. Li, T. Yang, X. Fan, G. Wu, Combined application of anti-VEGF and anti-EGFR attenuates the growth and angiogenesis of colorectal cancer mainly through suppressing AKT and ERK signaling in mice model, BMC Cancer 16 (2016) 791. https://doi.org/10.1186/s12885-016-2834-8.
[44] R. Jaafar, K. Mnich, S. Dolan, J. Hillis, A. Almanza, S.E. Logue, A. Samali, A.M. Gorman, RIP2 enhances cell survival by activation of NF-κB in triple negative breast cancer cells, Biochem. Biophys. Res. Commun. 497 (2018) 115–121. https://doi.org/10.1016/j.bbrc.2018.02.034.
[45] S.M. Singel, K. Batten, C. Cornelius, G. Jia, G. Fasciani, S.L. Barron, W.E. Wright, J.W. Shay, Receptor-interacting protein kinase 2 promotes triple-negative breast cancer cell migration and invasion via activation of nuclear factor-kappaB and c-Jun N-terminal kinase pathways, Breast Cancer Res. BCR 16 (2014) R28. https://doi.org/10.1186/bcr3629.
[46] A. Zare, A. Petrova, M. Agoumi, H. Amstrong, G. Bigras, K. Tonkin, E. Wine, S. Baksh, RIPK2: New Elements in Modulating Inflammatory Breast Cancer Pathogenesis, Cancers 10 (2018) 184. https://doi.org/10.3390/cancers10060184.
[47] L.P. Garo, A.K. Ajay, M. Fujiwara, G. Gabriely, R. Raheja, C. Kuhn, B. Kenyon, N. Skillin, R. Kadowaki-Saga, S. Saxena, G. Murugaiyan, MicroRNA-146a limits tumorigenic inflammation in colorectal cancer, Nat. Commun. 12 (2021) 2419. https://doi.org/10.1038/s41467-021-22641-y.
[48] M. Lethier, K. Huard, M. Hons, A. Favier, B. Brutscher, E. Boeri Erba, D.W. Abbott, S. Cusack, E. Pellegrini, Structure shows that the BIR2 domain of E3 ligase XIAP binds across the RIPK2 kinase dimer interface, Life Sci. Alliance 6 (2023) e202201784. https://doi.org/10.26508/lsa.202201784.
[49] F. Cipriani, M. Röwer, C. Landret, U. Zander, F. Felisaz, J.A. Márquez, CrystalDirect: a new method for automated crystal harvesting based on laser-induced photoablation of thin films, Acta Crystallogr. D Biol. Crystallogr. 68 (2012) 1393–1399. https://doi.org/10.1107/S0907444912031459.
[50] O. Svensson, S. Malbet-Monaco, A. Popov, D. Nurizzo, M.W. Bowler, Fully automatic characterization and data collection from crystals of biological macromolecules, Acta Crystallogr. D Biol. Crystallogr. 71 (2015) 1757–1767. https://doi.org/10.1107/S1399004715011918.
[51] C. Vonrhein, C. Flensburg, P. Keller, A. Sharff, O. Smart, W. Paciorek, T. Womack, G. Bricogne, Data processing and analysis with the autoPROC toolbox, Acta Crystallogr. D Biol. Crystallogr. 67 (2011) 293–302. https://doi.org/10.1107/S0907444911007773.
[52] A.J. McCoy, R.W. Grosse-Kunstleve, P.D. Adams, M.D. Winn, L.C. Storoni, R.J. Read, Phaser crystallographic software, J. Appl. Crystallogr. 40 (2007) 658–674. https://doi.org/10.1107/S0021889807021206.
[53] F. Long, R.A. Nicholls, P. Emsley, S. Graæulis, A. Merkys, A. Vaitkus, G.N. Murshudov, AceDRG: a stereochemical description generator for ligands, Acta Crystallogr. Sect. Struct. Biol. 73 (2017) 112–122. https://doi.org/10.1107/S2059798317000067.
[54] M.D. Winn, C.C. Ballard, K.D. Cowtan, E.J. Dodson, P. Emsley, P.R. Evans, R.M. Keegan, E.B. Krissinel, A.G.W. Leslie, A. McCoy, S.J. McNicholas, G.N. Murshudov, N.S. Pannu, E.A. Potterton, H.R. Powell, R.J. Read, A. Vagin, K.S. Wilson, Overview of the CCP4 suite and current

developments, Acta Crystallogr. D Biol. Crystallogr. 67 (2011) 235–242. https://doi.org/10.1107/S0907444910045749.
[55] G.N. Murshudov, A.A. Vagin, E.J. Dodson, Refinement of macromolecular structures by the maximum-likelihood method, Acta Crystallogr. D Biol. Crystallogr. 53 (1997) 240–255. https://doi.org/10.1107/S0907444996012255.
[56] P. Emsley, K. Cowtan, Coot: model-building tools for molecular graphics, Acta Crystallogr. D Biol. Crystallogr. 60 (2004) 2126–2132. https://doi.org/10.1107/S0907444904019158.
[57] V.B. Chen, W.B. Arendall, J.J. Headd, D.A. Keedy, R.M. Immormino, G.J. Kapral, L.W. Murray, J.S. Richardson, D.C. Richardson, MolProbity: all-atom structure validation for macromolecular crystallography, Acta Crystallogr. D Biol. Crystallogr. 66 (2010) 12–21. https://doi.org/10.1107/S0907444909042073.